Finite Element Simulation and Control of Nonlinear Flow and Reactive Transport

Ph.D Seminar

Andréa M. P. Valli

December, 1998

Adviser: *Álvaro L.G.A. Coutinho*

Co-adviser: *Graham F. Carey*

Contents

Chapter 1

Introduction

In the last two decades there has been a rapid expansion of research and applications for finite element simulations of fluid flow problems and transport processes. The maturation of the subject and the increasing power of computers enable the method to be applied a wide variety of flow problems. There are applications ranging from viscous incompressible non-newtonian flows to chemically reacting compressible high speed aerodynamic flows, and also diverse applications to complex fluid flow and species transport. For general treatments of the method see, for instance, Carey and Oden [3].

The need to develop improved algorithms has increased with the complexity of research applications. For instance, several adaptive time-stepping strategies have been studied as a means to provide solutions of complex coupled problems more efficiently. Errors and computational efficiency in transient (and steady state) solutions can be controlled using an automatic timestep selection strategy.

Adaptive techniques for automatic timestep determination are usually based on approximate local truncation error measures or on purely heuristic considerations. Winget and Hughes [21], Johan *et al.* [14], and Jacob and Ebecken [13] develop stepsize selections based on heuristic rules for transient heat conduction, compressible Navier-Stokes flows and structural dynamics problems, respectively. We remark that adaptive timestep selection can be viewed as an example of a feedback control problem [11, 12].

Schemes based on control theory used feedback from the computed solution to select the new timestep in accordance with a desired accuracy. In general, the timestep selection schemes are based on the control of maximum change in the key variables (pressure, concentration, velocities, etc.).

Coutinho and Alves [4] use this approach in their work of finite element simulation of fluid displacements in porous media. In the present studies we address the utilization of feedback control algorithms in conjunction with finite element analysis for flow and reactive transport problems.

Control theory has been extensively developed, particularly in electrical engineering and is also used widely in chemical engineering applications. Simple feedback control laws has been used with success to suppress the vortex shedding behind a circular cylinder [17, 10]. Recently, interest has increased in optimal flow control of viscous flows [20, 8, 9]. These problems own their complexity because of the highly nonlinear constraints given by approximations of the Navier-Stokes equations. To have an efficient computational tool for flow control or optimization, they use techniques to reduce the size of the problem to low-order systems models. The potential of control theory in conjunction with finite elements is obvious, and yet there have been relatively few focussed studies in this direction.

The focus in our work is the use of a Proportional-Integral-Differential (PID) control approach for automatic timestep selection. We also design a PID controller to solve a simple chemically reacting system through automatic feedback control applied to boundary conditions. No attempt is made to design an optimal feedback control law. The class of problems under investigation arise from coupled incompressible viscous flow and nonlinear transient heat or mass transfer. The finite element flow formulation is based on a penalty Galerkin method and the nonlinear reactive transport application utilizes a Galerkin approach.

The outline of the treatment is as follows. In the next chapter we presented the class of coupled flow and transport problems under investigation. The finite element formulation and solution approach is also given. Then, in chapter 3 we describe a simple PID control approach and indicate how it can be applied to timestep control and boundary control. Following this, a representative test problem for 2D coupled viscous flow and reactive transport is stated and results compared for fixed timestep, an adaptative timestep scheme in the literature and our PID control approach. Flow and species concentration results at the final time are also given. In section 4.2 we discuss isothermal reaction inside a porous catalyst. Next, we apply the timestep control algorithm to a highly nonlinear process on a catalyst section with heat effects included, and we show a simple example to test our boundary control approach. Finally, we summarize the main conclusions of this work in the last chapter.

Chapter 2

Coupled Viscous Flow and Transport

We are investigating applications arising in analysis of coupled incompressible viscous flow and heat or mass transfer. In the present work the class of problems under investigation will be restricted to transient Stokes flow and coupled transient reaction-convection-diffusion processes. The algorithm employs a decoupled scheme, where the Stokes equations are solved first, in each timestep. Then concentrations and temperatures are calculated, with the velocities as input in the transport equations. The finite element flow formulation is based on a penalty Galerkin method and the nonlinear reactive transport application utilizes a Galerkin approach.

The flow is determined by approximate solution of the classical unsteady Stokes problem: find the velocity-pressure pair ($\mathbf{u}$,p) satisfying

$$\frac{\partial \mathbf{u}}{\partial t} - \nu \Delta \mathbf{u} + \boldsymbol{\nabla} p = \mathbf{f} \tag{2.1}$$

$$\boldsymbol{\nabla} \cdot \mathbf{u} = 0 \tag{2.2}$$

with initial conditions

$$\mathbf{u}(\mathbf{x}, 0) = \mathbf{u}_0(\mathbf{x}) \quad \text{in } \Omega \tag{2.3}$$

and subject to prescribed boundary conditions

$$\mathbf{u} = \hat{\mathbf{u}} \quad \text{on } \partial\Omega \times [0, T]. \tag{2.4}$$

Here $\mathbf{f}$ is the applied body force, $\nu > 0$ is the kinematic viscosity, Ω is an open bounded domain in $\mathbb{R}^2$ with sufficiently smooth boundary $\partial\Omega$, T is a specified time, and the fluid density has been incorporated in p.

The transient transport equation is

$$\frac{\partial \mathbf{c}}{\partial t} + \mathbf{u} \cdot \boldsymbol{\nabla} \mathbf{c} - \boldsymbol{\nabla} \cdot (\mathbf{k} \boldsymbol{\nabla} \mathbf{c}) = \mathbf{g}(\mathbf{c}) \quad \text{in } \Omega \text{ and } t > 0 \tag{2.5}$$

with initial condition

$$\mathbf{c}(\mathbf{x}, 0) = \mathbf{c}_0(\mathbf{x}) \tag{2.6}$$

and boundary conditions for species concentration and flux

$$\mathbf{c} = \hat{\mathbf{c}} \qquad \text{on } \partial\Omega_1 \tag{2.7}$$

$$-\mathbf{k}\frac{\partial \mathbf{c}}{\partial n} = \beta(\mathbf{c} - \boldsymbol{\gamma}) \text{ on } \partial\Omega_2 \tag{2.8}$$

where $\mathbf{c}$ is the concentration vector of component species (including temperature), $\mathbf{u}$ is the velocity tensor, $\mathbf{k}$ is the diffusion tensor, $\mathbf{g}(\mathbf{c})$ is the chemical reaction source/sink term, and γ is a known value of the concentration vector in the medium. From (2.5) it is clear that the time rate of change (evolution) of the species component fields depends on advection, diffusion and chemical reaction, respectively. Here we assume that convective and diffusive effects are of the same order.

2.1 Penalty Finite Element Formulation for Stokes Problem

For simplicity and convenience we use a penalty method to enforce the incompressibility constraint. The penalty approach for the Stokes problem is designed to determine an approximate formulation involving only velocities and not pressures. Hence the size of the problem is reduced accordingly. The divergence-free condition $\nabla \cdot \mathbf{u} = 0$ is viewed as a constraint condition embedded in the variational problem by using a penalty term.

The classical approach for formulating variational problems with constraints is by use of Lagrange multiplies. We may obtain the penalized variational formulation of the Stokes problem by introducing the perturbed Lagrangian

$$L(\mathbf{u}, p) = \int_\Omega (\frac{\partial \mathbf{u}}{\partial t} \cdot \mathbf{u} \; + \; \frac{\nu}{2} \nabla \mathbf{u} \mathbf{:} \nabla \mathbf{u} \; - \; p \nabla \cdot \mathbf{u} \; - \; \frac{\epsilon}{2} p^2 \; - \; \mathbf{f} \cdot \mathbf{u}) \, dx \tag{2.9}$$

where ϵ is the penalized parameter ($0 < \epsilon \ll 1$), and the expression $\nabla\mathbf{u}{:}\nabla\mathbf{u}$ represents the dyadic product. Taking variations with respect to $\mathbf{u}$ at the stationary point ($\mathbf{u}$,p) and setting $\delta L = 0$, we get

$$\int_\Omega (\frac{\partial \mathbf{u}}{\partial t} \cdot \mathbf{v} \ + \ \nu \nabla\mathbf{u}{:}\nabla\mathbf{v} \ - \ p\nabla\cdot\mathbf{v} \ - \ \frac{\epsilon}{2}p^2 \ - \ \mathbf{f}\cdot\mathbf{v})\, dx = 0 \tag{2.10}$$

for arbitrary admissible $\mathbf{v} = \delta\mathbf{u}$. Now, if we take variations with respect to p at ($\mathbf{u}$,p), and we set $\delta L = 0$ for arbitrary admissible $q = \delta p$, we have

$$\int_\Omega (-\epsilon p \ - \ \nabla\mathbf{u})\, q \ dx = 0. \tag{2.11}$$

From equation (2.11) we see that the pressure approximation for the penalty formulation follows as

$$p^\epsilon = -\frac{1}{\epsilon}\nabla\mathbf{u}^\epsilon, \tag{2.12}$$

where $\mathbf{u}^\epsilon$ is the solution to the penalty problem.

The penalty form can be obtained substituting p^ϵ in (2.10): find $\mathbf{u}^\epsilon \in V$ satisfying the initial condition with $\mathbf{u}^\epsilon = \mathbf{g}$ on $\partial\Omega$ such that

$$\int_\Omega (\frac{\partial \mathbf{u}^\epsilon}{\partial t} \cdot \mathbf{v} \ + \ \nu \nabla\mathbf{u}^\epsilon{:}\nabla\mathbf{v} \ + \frac{1}{\epsilon}(\nabla\cdot\mathbf{u}^\epsilon)(\nabla\cdot\mathbf{v}))\, dx = \int_\Omega \mathbf{f}\cdot\mathbf{v}\, dx, \tag{2.13}$$

for all admissible $\mathbf{v} \in V$ with $\mathbf{v} = \mathbf{0}$ on $\partial\Omega$. For sufficient regular data $\mathbf{f}$, we can prove that as $\epsilon \to 0$, $\mathbf{u}^\epsilon$ will converge to $\mathbf{u}$, and p^ϵ will converge to the pressure p. For a discussion of existence and uniqueness see, e.g., [3].

Consider now approximation of the variational problem (2.13) using finite elements. Let $V^h \subset V$ be the finite element approximation space for velocities. In the usual way, the flow domain Ω is discretized to a union Ω_h of elements Ω_e, e = 1,2,...,E. Lagrange piecewise polynomials are used as global basis functions ϕ_j, j = 1,2,...,N, for the approximate subspace V^h. In this study we use continuous piecewise bilinear and piecewise biquadratic basis functions defined on a uniform discretization Ω_h of rectangular elements.

The direct approximation of the penalized variational problem (2.13) is to find $\mathbf{u}^\epsilon \in V^h$ satisfying the initial condition such that

$$\int_\Omega (\frac{\partial \mathbf{u}_h^\epsilon}{\partial t}\cdot\mathbf{v}_h + \nu\nabla\mathbf{u}_h^\epsilon{:}\nabla\mathbf{v}_h + \frac{1}{\epsilon}(\nabla\cdot\mathbf{u}_h^\epsilon)(\nabla\cdot\mathbf{v}_h))\, dx = \int_\Omega \mathbf{f}\cdot\mathbf{v}_h\, dx \quad \text{for all } \mathbf{v}_h \in V^h \tag{2.14}$$

with pressure approximation given by

$$p_h^\epsilon = -\frac{1}{\epsilon}\nabla \mathbf{u}_h^\epsilon. \tag{2.15}$$

Introducing the approximation

$$u_{jh}^e(\mathbf{x}) = \sum_{s=1}^{N} u_s^j \phi_s(\mathbf{x}), \tag{2.16}$$

for the components u_j^ϵ of the velocity and using $\boldsymbol{\omega}_h = (\phi_r, 0)$ and $(0, \phi_r)$ at interior node r, we have the following finite element system

$$\bar{\mathbf{M}}\frac{d\mathbf{u}^*}{dt} + \nu\bar{\mathbf{A}}\mathbf{u}^* + \frac{1}{\epsilon}\bar{\mathbf{B}}\mathbf{u}^* = \bar{\mathbf{F}} \tag{2.17}$$

where $\mathbf{u}^* = (\mathbf{u}_1, \mathbf{u}_2)^T$, and

$$\bar{\mathbf{M}} = \begin{bmatrix} \mathbf{M} & \mathbf{0} \\ \mathbf{0} & \mathbf{M} \end{bmatrix} \quad \bar{\mathbf{A}} = \begin{bmatrix} \mathbf{A} & \mathbf{0} \\ \mathbf{0} & \mathbf{A} \end{bmatrix} \quad \bar{\mathbf{B}} = \begin{bmatrix} \mathbf{B}_x & \mathbf{B}_{xy} \\ \mathbf{B}_{xy}^T & \mathbf{B}_y \end{bmatrix} \quad \bar{\mathbf{F}} = \begin{bmatrix} \mathbf{F}_x \\ \mathbf{F}_y \end{bmatrix}$$

with

$$\begin{aligned}
m_{ij} &= \int_{\Omega_h} \phi_i \phi_j \, dx \\
a_{ij} &= \int_{\Omega_h} ((\phi_i)_x(\phi_j)_x + (\phi_i)_y(\phi_j)_y) \, dx \\
(b_x)_{ij} &= \int_{\Omega_h} (\phi_i)_x(\phi_j)_x \, dx \\
(b_{xy})_{ij} &= \int_{\Omega_h} (\phi_i)_x(\phi_j)_y \, dx \\
(b_y)_{ij} &= \int_{\Omega_h} (\phi_i)_y(\phi_j)_y \, dx \\
(f_x)_i &= \int_{\Omega_h} f_1 \phi_i \, dx \qquad (f_y)_i = \int_{\Omega_h} f_2 \phi_i \, dx.
\end{aligned} \tag{2.18}$$

If the penalty term in (2.17) is integrated exactly then the method will not yield solutions $\mathbf{u}_h^\epsilon$ that converge to $\mathbf{u}_h$ as $\epsilon \to 0$. The velocity field $\mathbf{u}_h^\epsilon \to 0$ as $\epsilon \to 0$ and the constraint equation $\nabla \cdot \mathbf{u} = 0$ dominates in this limit. The discrete finite element solution is said to "lock" [see, e.g.,[22],[16],[15]]. To obtain an approximate solution other than the "locking" solution, we use reduced integration for evaluating the penalty integral. The penalty term is

approximately integrate using a Gauss quadrature rule of lower order than that required for exact integration.

If we denote $I(\cdot)$ the reduced quadrature rule for the penalty integration, the penalty term in (2.17) is given by

$$\frac{1}{\epsilon}\bar{\mathbf{B}}\mathbf{u}^* = \frac{1}{\epsilon}\int_{\Omega_h} I\left(\nabla\cdot\mathbf{u}_h^\epsilon\,\nabla\cdot\mathbf{v}_h\right)\,dx. \tag{2.19}$$

In the numerical studies we consider two special cases: continuous piecewise bilinear basis of the 4-node bilinear rectangle with one-point Gauss quadrature rule for the penalty term (2.19) and continuous piecewise biquadratic basis of the 9-node biquadratic rectangle with (2×2) Gauss quadrature rule for the penalty term (2.19).

The semidiscrete Stokes's system is integrate implicitly using a Crank-Nicolson scheme with timestep $\triangle t$. At each timestep we have to solve a linear system of the form

$$\mathbf{P}\mathbf{u}^*_{n+1} = \mathbf{d} \tag{2.20}$$

where

$$\begin{aligned}\mathbf{P} &= \bar{\mathbf{M}} + \frac{\triangle t}{2}(\nu\bar{\mathbf{A}} + \frac{1}{\epsilon}\bar{\mathbf{B}})\\ \mathbf{d} &= (\bar{\mathbf{M}} - \frac{\triangle t}{2}(\nu\bar{\mathbf{A}} + \frac{1}{\epsilon}\bar{\mathbf{B}}))\mathbf{u}^*_n + \frac{\triangle t}{2}\,(\frac{\bar{\mathbf{F}}_{n+1}+\bar{\mathbf{F}}_n}{2})\end{aligned}$$

and n denotes the time index.

2.2 Finite Element Formulation for the Transport Equation

To find approximate solutions for the transport problem corresponding to (2.5)-(2.8), we use a traditional Galerkin finite element formulation. For simplicity we show the formulation for the particular case of one transport component c. The extension to the case of more than one species is not difficult. We can handle up to nine different species in our code.

A week variational statement may be obtained by integration by parts of the diffusion term in a standard residual formulation, and then using the Gauss divergent theorem. The variational problem reduces to solving for c

satisfying the initial conditions such that

$$\int_{\Omega}(\frac{\partial c}{\partial t}\omega+\mathbf{u}\cdot\nabla c\,\omega+\mathbf{k}\nabla c\cdot\nabla\omega)\;dx+\int_{\partial\Omega_2}\beta(c-\gamma)\omega\;ds=\int_{\Omega}g_i(c)\,\omega\;dx \quad (2.21)$$

for all admissible test functions $\omega \in H_0$.

We may construct a semidiscrete Galerkin finite element method introducing a spatial discretization and an appropriate finite element space for the admissible functions in (2.21). Let Ω_h denote the finite element discretization of Ω, and $H_0^h \subset H_0$ be the finite-dimensional subspace spanned by finite element basis ψ_i, i = 1,2,. . . ,N. The finite element problem is to find $c_h \in {H_0}^h$ satisfying the initial condition such that

$$\int_{\Omega_h}(\frac{\partial c_h}{\partial t}\omega_h+\mathbf{u}_h\cdot\nabla c_h\omega_h+k\nabla c_h\cdot\nabla\omega_h)dx+\int_{\partial\Omega_2}\beta(c_h-\gamma)\omega_h ds=\int_{\Omega_h}g_i(c)\omega_h dx \quad (2.22)$$

for all $\omega_h \in {H_0}^h$. The finite element approximation for the concentration c_h at any time t can be expressed as

$$c_h(\mathbf{x},t)=\sum_{j=1}^{N}c_j(t)\psi_j(\mathbf{x}) \quad (2.23)$$

where the nodal solution values c_j depend continuously on time. We have in this studies continuous piecewise basis functions defined by the 4-node bilinear rectangle, the 9-node biquadratic rectangle and the 6-node biquadratic triangle.

Introducing (2.23) into (2.22) and setting $\omega_h = \psi_i$, i = 1,2,. . . ,N, we have the resulting semi-discrete ODE system for the nodal vector $\mathbf{c}$

$$\mathbf{M}\frac{d\mathbf{c}}{dt}+\mathbf{B}(\mathbf{u})\,\mathbf{c}+\mathbf{D}\,\mathbf{c}=\mathbf{g}(c) \quad (2.24)$$

where

$$\begin{aligned} m_{ij} &= \int_{\Omega_h}\psi_i\psi_j\;dx \\ b_{ij} &= \int_{\Omega_h}\mathbf{u}\cdot\nabla\psi_j\psi_i\;dx \\ d_{ij} &= \int_{\Omega_h}k\nabla\psi_i\cdot\nabla\psi_j\;dx+\int_{\partial\Omega_2}\beta\psi_i\psi_j\;ds \\ g_i &= \int_{\Omega_h}g(c)\psi_i\;dx+\int_{\partial\Omega_2}\gamma\psi_i\;ds \end{aligned} \quad (2.25)$$

We integrate the ODE system implicitly using a Crank-Nicolson scheme with timestep $\triangle t$. Since the chemical reaction source term can be a nonlinear function of the unknown concentration, we have to solve at each timestep $\triangle t$ a nonlinear system of the form

$$\mathbf{F}(\mathbf{c}^{n+1}) = 0 \tag{2.26}$$

where

$$\mathbf{F}(\mathbf{c}^{n+1}) = (\mathbf{M} + \frac{\triangle t}{2}(\mathbf{B} + \mathbf{D}))\,\mathbf{c}^{n+1} \; - \; \frac{\triangle t}{2}\mathbf{g}(\mathbf{c}^{n+1}) + \mathbf{G}$$

with

$$\mathbf{G} = -\,(\mathbf{M} - \frac{\triangle t}{2}(\mathbf{B} + \mathbf{D}))\,\mathbf{c}^{n} \; - \; \frac{\triangle t}{2}\mathbf{g}(\mathbf{c}^{n})$$

and n denotes the timestep index.

The nonlinear system (2.26) is solved by Newton's method in the present study. If we define $\mathbf{U} = \mathbf{c}^{n+1}$, we construct and solve the linear system

$$\mathbf{J}(\mathbf{U}^{k+1} \; - \; \mathbf{U}^{k}) = -\,\tilde{\mathbf{F}} \tag{2.27}$$

where $\mathbf{U}^0$ is given, with

$$\mathbf{J} = (\mathbf{M} + \frac{\triangle t}{2}(\mathbf{B} + \mathbf{D})) \; - \; \frac{\triangle t}{2}\frac{\partial \mathbf{g}}{\partial \mathbf{U}}(\mathbf{U}^{k})$$

and

$$\tilde{\mathbf{F}} = (\mathbf{M} + \frac{\triangle t}{2}(\mathbf{B} + \mathbf{D}))\mathbf{U}^{k} \; - \; \frac{\triangle t}{2}\mathbf{g}(\mathbf{U}^{k}) \; + \; \mathbf{G}$$

for each iterate $\mathbf{U}^{k+1}$. Here the solution of the linear system (2.27) is also obtained using a frontal solver. The timestep may be chosen adaptively and in the next section we describe one possible strategy for timestep selection that utilizes a PID control scheme based on the approach in Coutinho and Alves [4].

Chapter 3

Adaptive Control

3.1 PID Control

Control can be defined as the process of making a system of variables follow a particular value, called the reference value. Closed-loop process control uses a measurement of the controlled variable and feedback of this signal to compare it with a reference value. The feedback is supplied from an output sensor of some sort, and feeds an input of the controller to tell the controller how far the output is from its reference value. The controller uses this information to correct the output error. This kind of process is used in applications ranging, for example, from air conditioning thermostats to guidance and control of aircraft.

A simple feedback system consists of an actuator, a control device often called controller, the process (or plant), and an output sensor, as shown in Figure 3.1. The central component of a feedback control system is the process, whose output is to be controlled. In our case we are interested in process control. The difference between the desired output and the actual output of the system measured by an sensor is equal to the error, which is adjusted by the controller. The actuator is the device that can influence the controlled variable of the process. The output of the control device causes the actuator to modulate the process in order to reduce the error.

One example of a feedback control system is the room-temperature control system of a house [7]. The plant is the house, the thermostat is the output sensor, the gas valve is the controller, and the furnace is the actuator. Suppose the thermostat is turned on when both the temperature in the house

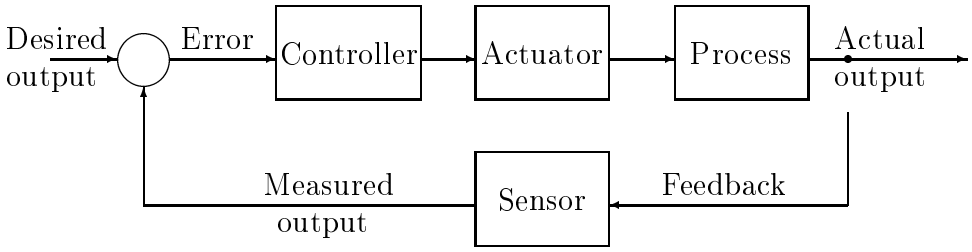

Figure 3.1: A feedback system block diagram of a basic closed-loop control system

and the outside temperature are below the reference temperature. The gas valve will be open causing the furnace to fire and heat to be supplied to the house. This is a closed loop system.

One of the most widely used algorithms for closed-loop control is the three-term control, known as the Proportional-Integral-Differential (PID) control loop. The popularity of PID controllers can be attributed to their functional simplicity and to their robust performance in a large range of operating conditions. The objective in using PID control algorithms is to control the output along a smooth curve (vs. time) towards the set-point while minimizing overshoot, the amount the system output response proceeds beyond the desire response.

A PID control algorithm includes a term which is proportional (P) to the output error, a term proportional to the integral (I) of the error, and a term proportional to the derivative (D) of the error, and therefore has the form

$$-S(\tau) = k\left\{\theta(\tau) + \frac{1}{T_I}\int_0^{\tau}\theta(\tilde{\tau})d\tilde{\tau} + T_D\frac{d\theta(\tau)}{d\tau}\right\} \tag{3.1}$$

or

$$-\dot{S}(\tau) = k_I\theta(\tau) + k_P\dot{\theta}(\tau) + k_D\ddot{\theta}(\tau) \tag{3.2}$$

where $S(\tau)$ is the controller output deviation, $\dot{S}(\tau)$ implies time rate of change of S, $\theta(\tau)$ is the error, k is the proportional gain, T_I is called the integral, or reset time, T_D is the derivative time, and k_I, k_P and k_D are the integral, proportional and derivative parameters, respectively. In order to adapt the continuous-time model to a discrete environment, we replace

derivatives by differences in (3.2) to obtain:

$$-(S_{n+1} - S_n) = k_I\,\theta_n + k_P\,(\theta_n - \theta_{n-1}) + k_D\,(\theta_n - 2\theta_{n-1} + \theta_{n-2}) \qquad (3.3)$$

The proportional term acts like a rubber band in an analogous mechanical system: it exerts a restoring force proportional to how much the rubber band is stretched from its original shape. The proportional term can reduce error responses to disturbances as we adjust k_D up or down. The integral term is added to reduce or eliminate constant steady state errors. It can do this because it sums up errors over time. The derivative feedback is used in conjunction with proportional and/or integral feedback to increase the damping of the dynamic response. In general, it also improves the stability of the system. These three kinds of control attempt to provide a good degree of error reduction simultaneously with acceptable stability and damping.

Designing a particular PID control loop requires merely tuning the controller. The constants k_P, k_I, and k_D have to be adjust to yield satisfactory control. Increasing k_P and k_I tends to reduce system errors but may lead to instability, while increasing k_D tends to improve stability. The selection of the parameters is basically a search in a three-dimensional space. There are several methods and rules proposed to solve this parameter selection problem. Dorf and Bishop, [5], for instance, show many design methods using root locus and performance indices. In the next section we describe one possible strategy that utilizes a discrete PID control scheme for automatic timestep selection based on the approach in Coutinho and Alves, [4].

3.2 Timestep Control

The particular problems considered here arise from coupled incompressible viscous flow and nonlinear transient heat or mass transfer. The nonlinearity enters through a chemical reaction source or sink term in the transport equation. Depending on the nature of the data and nonlinearity, we may need to choose a very small timestep to obtain convergence in solving the nonlinear system (2.26). In general the problem occurs in the beginning of the implicit time integration scheme. To increase the robustness of our time scheme we use adaptive timestep selection based on feedback control theory.

Many studies have been made to improve stepsize selection in numerical integration of ordinary differential equations; e.g. in the finite element field we can find timestep selection strategies based on heuristic rules such as in

Winget and Hughes, [21], for transient heat conduction. Gustaffson *et al.*, [11], and Hairer and Wanner, [12], viewed the problem of automatic timestep selection as examples of feedback control problems. This approach was used by Coutinho and Alves, [4], in their work of finite element simulation of miscible displacements in porous media.

Most timestep schemes are based on controlling accuracy as determined by truncation error estimates (e.g. Prediction-Modification-Correction). The objective of timestep selection is to minimize the computational effort to construct an approximate solution of a given problem in accordance with a desired accuracy. In general, timestep selection can be expressed as

$$\triangle t_{n+1} = \left(\frac{tol}{e_n}\right) \triangle t_n \tag{3.4}$$

which can be rewritten as

$$-\left(\log \triangle t_{n+1} - \log \triangle t_n\right) = \left(\log e_n - \log tol\right) \tag{3.5}$$

where tol is some input tolerance, e_n is an estimate of the local truncation error, and $\triangle t_n$ is the timestep in the previous iteration. Equation (3.5) is equivalent to equation (3.2) if we take $k_P = k_D = 0$, $k_I = 1$, and

$$S_n = \log \triangle t_n \tag{3.6}$$

$$\theta_n = \log e_n - \log tol \tag{3.7}$$

Thus, the timestep selection strategy (3.4) can be interpreted as a simplified version of the standard integral feedback controller. We recognize $\log \triangle t_n$ as the control variable, the deviation $(\log e_n - \log)$ as the control error, and $\log tol$ as the set point.

Figure (3.2) shows a block diagram of the feedback control problem. The process takes the timestep $\triangle t_n$ as a input, calculates the solution of the problem, and produces an error estimate e_n that is fed back to the controller. The controller tries to select the new timestep in a such way that the quantity $\log e_n$ comes as close as possible to $\log tol$.

Using these ideas we can design a new stepsize control algorithm using the standard discrete PID controller (3.3),

$$-(S_{n+1} - S_n) = k_I\, \theta_n + k_P\, (\theta_n - \theta_{n-1}) + k_D\, (\theta_n - 2\theta_{n-1} + \theta_{n-2}).$$

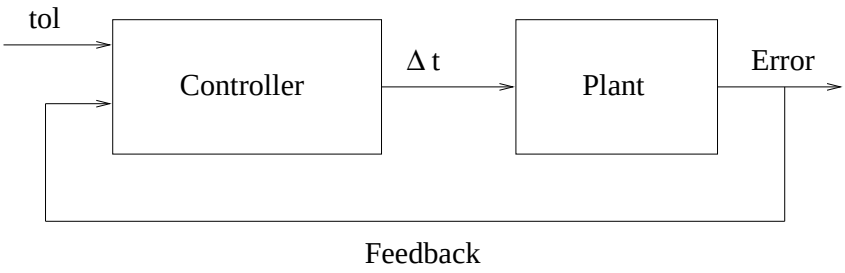

Figure 3.2: Stepsize selection viewed as a control problem.

Substituting the definitions (3.6) and (3.7) into the above equation, we have

$$\begin{aligned} -(\log \triangle t_{n+1} - \log \triangle t_n) \;\; = \;\; & k_I(\log e_n - \log tol) \; + \\ & k_P\left[(\log e_n - \log tol) - (\log e_{n-1} - \log tol)\right] \; + \\ & k_D\left[(\log e_n - \log tol) - 2(\log e_n - \log tol) \; + \right. \\ & \left. \quad (\log e_n - \log tol)\right] \end{aligned}$$

which can be rearranged as,

$$\triangle t_{n+1} = (\frac{e_{n-1}}{e_n})^{k_P}(\frac{tol}{e_n})^{k_I}(\frac{{e_{n-1}}^2}{e_n e_{n-2}})^{k_D} \; \triangle t_n, \tag{3.8}$$

where tol is some input tolerance, e_n is the measure of the change of the quantities of interest in time step $\triangle t_n$, and k_P, k_I and k_D are the PID parameters.

An estimate of the solution change is compared with the specified accuracy requirement, and the result is fed back to calculate the new time step. The controller tries to select the stepsize such that e_n comes as close as possible to the input tolerance, tol, along a smooth curve. Figure (3.3) shows a flow chart of our PID control algorithm. For time step n = 2, 3, ... we may proceed sequentially as follows:

1. Given $(\triangle t)_{min}$, $(\triangle t)_{max}$, k_P, k_I, k_D, and tol, and starting with e_{n-2}/tol $= e_{n-1}/tol = 1.0$, and $\triangle t_{n+1} = \triangle t_n =$ some initial timestep value.

2. calculate e_n.

3. if $e_n > tol$ reject the timestep:

   - $t^{n+1} = t^n$ - $\triangle t_n$

- $\triangle t_{n+1} = \max\,(\frac{tol}{e_n}\triangle t_n,\, \triangle t_{min})$
- $c^{n-1} \leftarrow c^n$

else

- calculate $\triangle t_{n+1}$ using (3.8)
- $\triangle t_{n+1} = \max\,(\triangle t_{n+1},\, \triangle t_{min})$
- $\triangle t_{n+1} = \min\,(\triangle t_{n+1},\, \triangle t_{max})$

4. $e_{n-2} = e_{n-1},\, e_{n-1} = e_n$.

In the present work the measure of the relative change e_n of the solution (e.g. concentration, temperature, velocities) over a timestep is evaluate by computing $\frac{\|\mathbf{c}^{n+1}-\mathbf{c}^n\|}{\|\mathbf{c}^{n+1}\|}$, where c^n is the approximate solution at time t^n, and $\|\cdot\|$ denotes the Euclidean norm. We supply timestep limits, $(\triangle t)_{min}$ and $(\triangle t)_{max}$, to incorporating the anti_windup effect, according to control theory [5].

If a timestep gives an unacceptable value of e_n, the step is rejected. Then the step is repeated with a scaled timestep size based on the magnitude of the error relative to the tolerance. However, we find in numerical experiments that the number of rejections is very small, producing a smooth sequence of timesteps as we will see in chapter 4. In our algorithm, if the sequence of iterates of the nonlinear system is converging at a slow rate, the timestep is also rejected.

Although feedback control theory provides sophisticated techniques to choose the PID parameters, robustness is required when a general finite element method is used for a wide range of different simulations. We perform parametric studies of the PID controller for values similar to those used by Gustaffson *et al.* [11] and also by Coutinho and Alves [4]. Subsequent numerical experiments demonstrate that the PID controller is very robust for the reaction-diffusion applications studied here.

In the next section we use the ideas developed here to solve a simple chemically reacting system through automatic feedback control applied to boundary conditions. We discuss the algorithm implementation and later the limitations of PID controllers to solve more complex boundary control problems.

Algorithm:

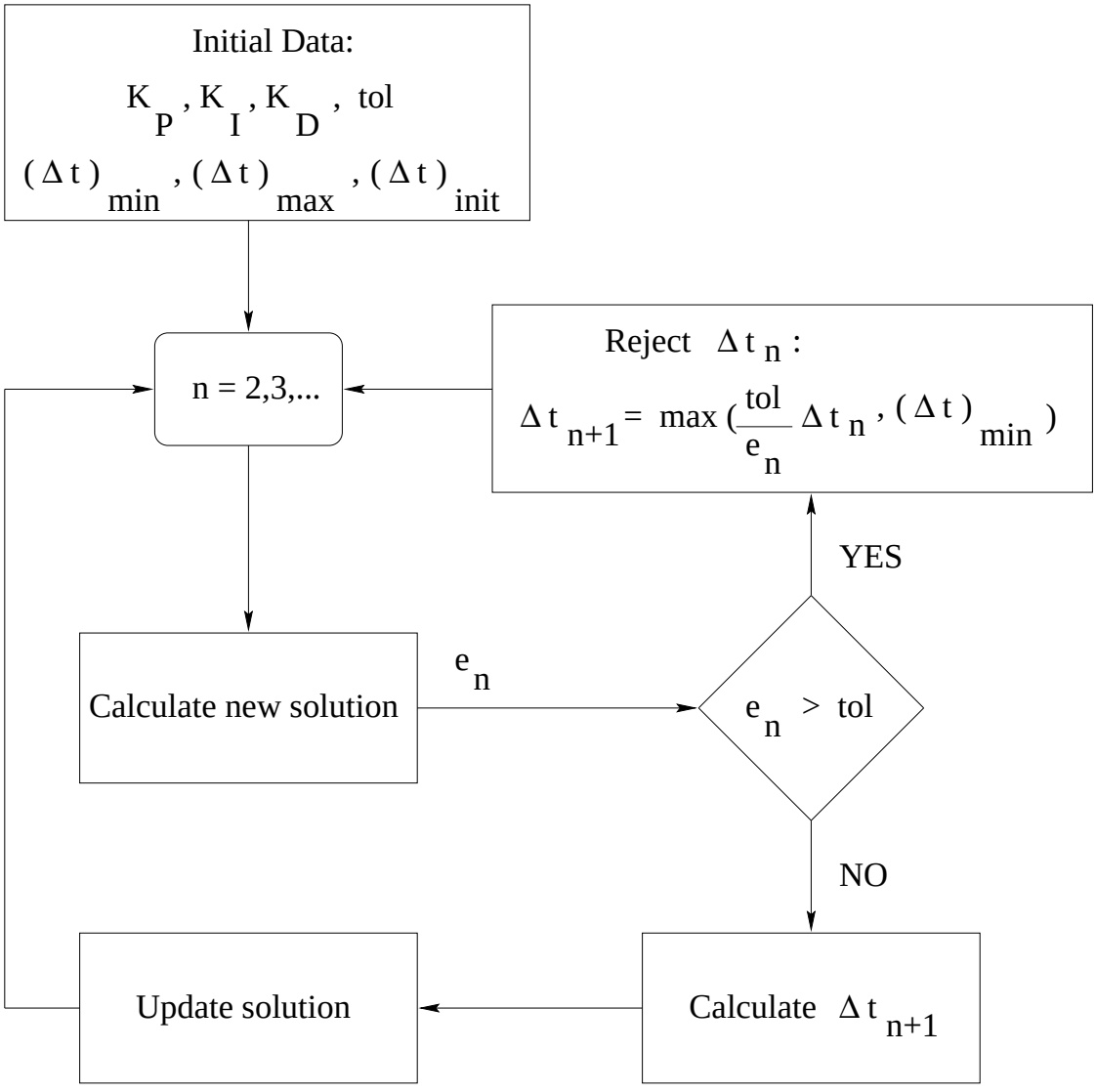

Figure 3.3: The flow chart of the PID control algorithm.

3.3 Boundary Control

Consider the steady state solution for coupled chemical reaction with heat transfer. The control problem is to find the value of the temperature or concentration on portions of the boundary that keeps the temperature or concentration at a specified point of the domain as close as possible of a target value. The control variable is the step in the boundary condition, δbc_m, and the quantity to be controlled is the difference between the temperature or concentration at $\hat{\mathbf{x}}$ and some target value. Using the same notation as before, we have

$$S_m = \delta bc_m \tag{3.9}$$

$$\theta_m = c_m^* - c_{targ} \tag{3.10}$$

where S_m is the control variable, θ_m is the deviation, $\hat{\mathbf{x}}$ is a fixed point in the domain, c_m^* is the approximate steady state temperature or concentration at $\hat{\mathbf{x}}$ calculate at iteration m, and c_{targ} is the target value.

To design our boundary control algorithm, we use again the standard discrete PID controller (3.3),

$$-(S_{m+1} - S_m) = k_I\,\theta_m + k_P\,(\theta_m - \theta_{m-1}) + k_D\,(\theta_m - 2\theta_{m-1} + \theta_{m-2}).$$

Substituting the definitions (3.9) and(3.10) into the above equation, we have

$$\delta bc_{m+1} = \delta bc_m - k_I(c_m^* - c_{targ}) - k_P(c_m^* - c_{m-1}^*) - k_D(c_m^* - 2c_{m-1}^* + c_{m-2}^*) \tag{3.11}$$

$$bc_{m+1} = bc_m + \delta bc_{m+1} \tag{3.12}$$

where bc_m is the value of the temperature or concentration on portions of the boundary, and k_I, k_P and k_D are the integral, proportional and derivative parameters. The boundary control process is summarized in the following algorithm:

1. Compute u and v according to (2.20).
2. Set $m = 0$ and $id_{stop} = 0$.
3. Assign values to δbc_m, bc_m, k_I, k_P, k_D, ϵ, m_{max}, c_{targ}, and $\hat{\mathbf{x}}$.
4. While $(id_{stop} = 0)$ and $(m \leq m_{max})$

- Compute the steady state temperature and concentration according to (2.27).
- Set c_m^* equal to the temperature or concentration at point $\hat{\mathbf{x}}$.
- Compute the error $= \frac{\|c_m^* - c_{targ}\|}{\|c_{targ}\|}$, and set $id_{stop} = 0$ if error $< \epsilon$
- Compute δbc_{m+1} and bc_{m+1} according to (3.11) and (3.12) , respectively.
- Impose the new boundary condition
- $m = m + 1$

In the boundary control process, we start the calculations of the new boundary condition using the control (3.11) when $m = 3$. In the first two iterations we increment the boundary condition using a given constant value.

Chapter 4

Numerical Results

4.1 Validation Problems

The first example is a particular test problem introduced by Johnson and Pitkaranta [15] for the Stokes flow (2.1)-(2.4), and also studied by Song et al. [19] and Carey and Krishnan [2]. The analytic solution for this problem is defined by the velocity vector field

$$\begin{aligned} u(x,y) &= x^2(1-x)^2(2y-6y^2+4y^3) \\ v(x,y) &= y^2(1-y)^2(-2x+6x^2-4x^3) \end{aligned} \tag{4.1}$$

and the pressure field

$$p(x,y) = x^2 - y^2 \tag{4.2}$$

on the unit square $\Omega = (0,1) \times (0,1)$. This velocity field is divergent free and satisfies the no-slip condition on $\partial\Omega$. Substituting (4.1) and (4.2) in the Stokes equation (2.1), we find that the body force $\mathbf{f} = (f_1, f_2)$ is equal to

$$\begin{aligned} f_1(x,y) &= 2x - 0.01[(2-12x+12x^2)(2y-6y^2+4y^3) + \\ &\quad (x^2-2x^3+x^4)(-12+24y)] \\ f_2(x,y) &= -2y - 0.04[(-x+3x^2-2x^3)(1-6y+6y^2) + \\ &\quad (3-6x)(1-y)^2y^2)]. \end{aligned}$$

The viscosity is chosen as 0.01 units, and we take a constant penalty parameter of $\epsilon = 10^{-8}$. The maximum nodal velocity is approximately 1.2×10^{-2} units, which corresponds to a Reynolds number of 1.2. The approximate solution is computed for a sequence of uniform meshes with mesh size $h =$

$\frac{1}{2}, \frac{1}{4}, \frac{1}{8}, \frac{1}{16}, \frac{1}{32}$, and all the approximations are shown for the first timestep 10^{-5}. The initial condition is taken as the exact solution at the initial time $t = 0$. Our objective is to examine the rates of convergence for this test problem, and to compare with the theoretical estimates.

Table 4.1 shows the error in the approximate velocity in the L^2-norm ($\|\cdot\|_0$) and H^1-norm ($\|\cdot\|_1$) for the refined meshes in Case 1 (bilinears). The error in the approximate velocity is plotted against mesh size h on a log-log scale in Figure 4.1. The respective approximate slopes of 1.9026 and 0.9797 indicate global rates of convergence. The theoretical rates of convergence in Case 1 in the $\|\cdot\|_0$ and $\|\cdot\|_1$ norms are equal to 2 and 1, respectively.

Mesh Size	L^2-norm	H^1-norm
h = 1/2	$.7746371089279643E-02$	$.5754132802187018E-01$
h = 1/4	$.2463945413680297E-02$	$.3099889670988598E-01$
h = 1/8	$.6504252528721037E-03$	$.1551477584896485E-01$
h = 1/16	$.1641288155366836E-03$	$.7734175790649037E-02$
h = 1/32	$.4107556219923611E-04$	$.3861947127641377E-02$

Table 4.1: The L^2-norm and H^1-norm of error in the velocity solution for bilinear elements.

The error in the velocity in the norms $\|\cdot\|_0$ and $\|\cdot\|_1$ in Case 2 (biquadratics) is shown in Table 4.2. Figure 4.2 shows the error in the approximate velocity plotted against mesh size h on a log-log scale. The slopes of the curves yield rates of convergence for the velocity 2.9628 and 2.0154 in the $\|\cdot\|_0$ and $\|\cdot\|_1$ norms , respectively. Hence we find that the velocity approximations in both cases converge towards the exact solution at optimal rates.

The second numerical experiment is a validation study for the transport equation (2.5)-(2.8). A test problem is constructed to have in the unit square domain and $t > 0$ analytic solution

$$c = 10^2(t+1)^2 x(x-1)y(y-1) \tag{4.3}$$

for concentration. The velocity field is the same used in the first example (4.1). We assume $k_{11} = k_{22} = 1$, $k_{12} = k_{21} = 0$, and the reaction term is taken to be

$$g(x,y) = -c^2 + f, \tag{4.4}$$

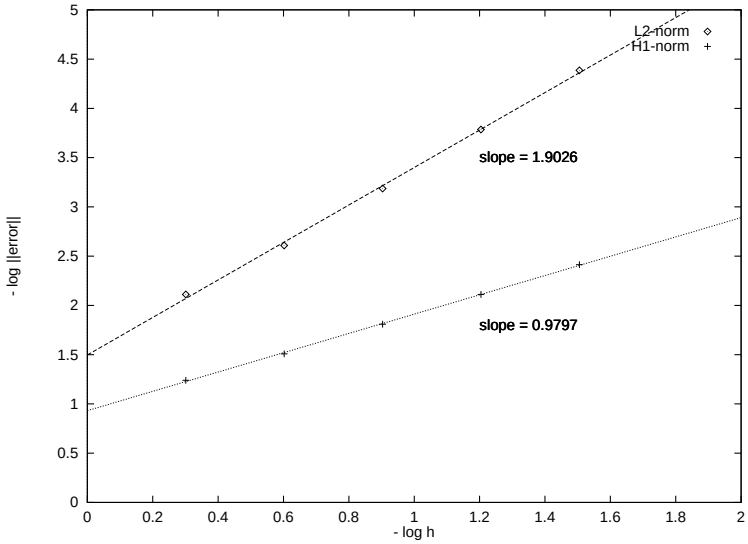

Figure 4.1: Optimal global rates of convergence for the velocity using biquadratic elements.

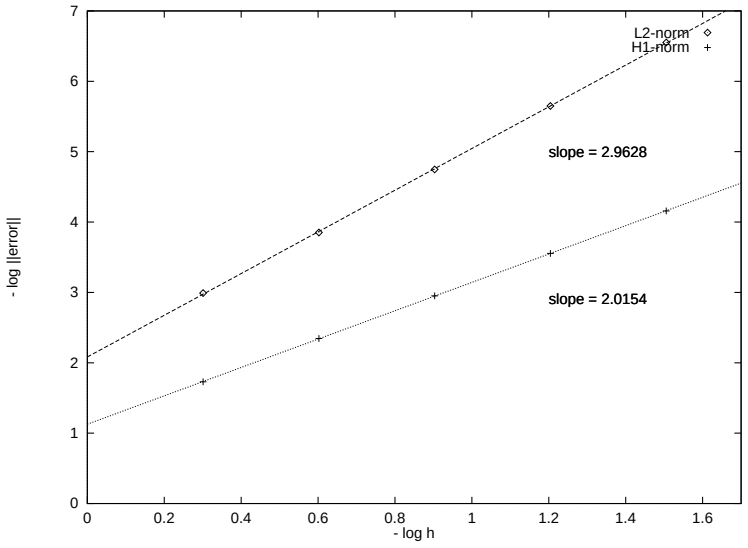

Figure 4.2: Optimal global rates of convergence for the velocity using biquadratic elements.

Mesh Size	L^2-norm	H^1-norm
h = 1/2	$.1021730098325111E-02$	$.1866760928638470E-01$
h = 1/4	$.1404786196967832E-03$	$.4521962356252536E-02$
h = 1/8	$.1786013086271515E-04$	$.1117877402750865E-02$
h = 1/16	$.2242721112992155E-05$	$.2786660995213754E-03$
h = 1/32	$.2806896476081326E-06$	$.6961697872977085E-04$

Table 4.2: The L^2-norm and H^1-norm of error in the velocity solution for biquadratic elements.

where the function f is given by

$$f = \frac{\partial c}{\partial t} + u\frac{\partial c}{\partial x} + v\frac{\partial c}{\partial y} - k_{11}\frac{\partial^2 c}{\partial x^2} - k_{22}\frac{\partial^2 c}{\partial y^2} + c^2.$$

The initial solution is defined as the exact solution at the initial time $t = 0$. We specify essential boundary conditions, $c(t, x, y) = 0$ from (4.3) evaluated on the boundary of the unit square domain Ω. Of particular interest here is to examine the rates of convergence of the concentration for this test problem and compare them with the theoretical estimates.

The transport equation is solved using the bilinear, biquadratic and six-node triangular elements described earlier for a sequence of uniform meshes with mesh size $h = \frac{1}{2}, \frac{1}{4}, \frac{1}{8}, \frac{1}{16}$, and $\frac{1}{32}$. In the case of bilinear elements, we also compute the solution at $h = \frac{1}{64}$. For the convergence study with respect to h we keep a constant small timestep of $\Delta t = 10^{-04}$. All the approximations are shown for the first time step $t = 10^{-04}$.

The L^2-norm of the error in the concentration solution for bilinear and six-node triangular elements is shown in Table 4.3. The L^2-norm and H^1-norm of the error for the concentration using bilinear elements are plotted against mesh size in Figure 4.3 on a log-log scale. The respective slopes 1.9708 and 1.0202 indicate the global rates of convergence, and are in good agreement with the theoretical predictions 2 and 1, respectively.

For biquadratic elements we obtain relative errors in the L^2-norm of order less than 10^{-14} for any number of elements. This means that within roundoff error we obtain the exact solution as expected.

Optimal global rates of convergence are also obtained for six-node triangular elements in both norms as shown in Figure 4.4. (The rates of convergence

Mesh Size	4-node bilinear	6-node triangular
h = 1/2	$.12873418E+01$	$.30613016E+00$
h = 1/4	$.35371359E+00$	$.43871262E-01$
h = 1/8	$.90379169E-01$	$.56366812E-02$
h = 1/16	$.22716094E-01$	$.70867673E-03$
h = 1/32	$.56865901E-02$	$.88027906E-04$

Table 4.3: The L^2-norm of the error in concentration for 4-node bilinear and 6-node triangular elements.

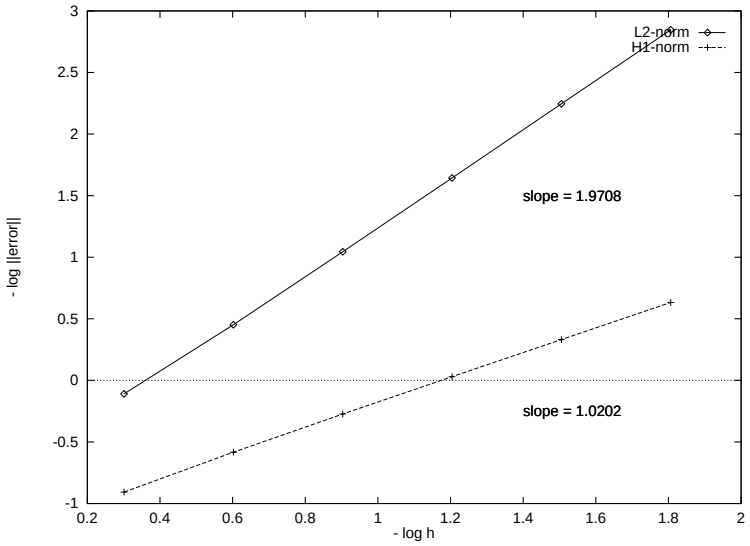

Figure 4.3: Rates of convergence for the concentration approximation in the L^2-norm and H^1-norm with bilinear functions

for the concentration approximation in the L^2-norm and H^1-norm for this example are 2.9480 and 1.9699, respectively.)

We also examined the order of convergence of the solution with respect to the time step Δt. In view of the above convergence results we select for this study biquadratic basis functions and a mesh with 2×2 elements. The approximate solutions are compared at the time $t = 0.1$ for values of Δt equal to $10^{-02}, 10^{-03}, 10^{-04}$ in Table 4.4. The error in the L^2-norm is plotted against Δt on a log-log scale in Figure 4.5. We know that the theoretical truncation error for the Crank-Nicolson scheme is $O(\Delta t^2)$, and we see an

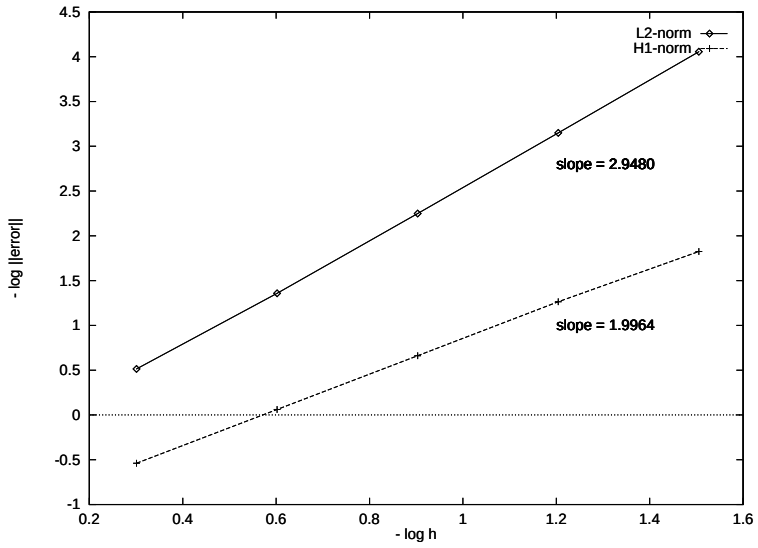

Figure 4.4: Rates of convergence for the concentration approximation in the L^2-norm and H^1-norm with six-node triangular elements

approximate slope of 2.0397.

Time Step Size	L^2-norm of the error
$\Delta t = 10^{-02}$	$.16462243E-01$
$\Delta t = 10^{-03}$	$.13438152E-03$
$\Delta t = 10^{-04}$	$.13711075E-05$

Table 4.4: The L^2-norm of error in the concentration solution for a mesh with 2×2 biquadratic elements.

Our main objective now is to assess the accuracy of the solutions when the time step control strategies studied previously are applied to the validation problem. In particular, we want to see if we can obtain approximate solutions of the same accuracy as before but with a small number of time steps. We also want to verify that the PID controller is robust.

To compare the PID timestep control and the strategy developed by Winget and Hughes [21] we again use a grid with 2 biquadratic elements as in the previous study for convergence of the Crank-Nicolson method. The initial time step size is 10^{-04}, and we allow a minimum and a maximum time

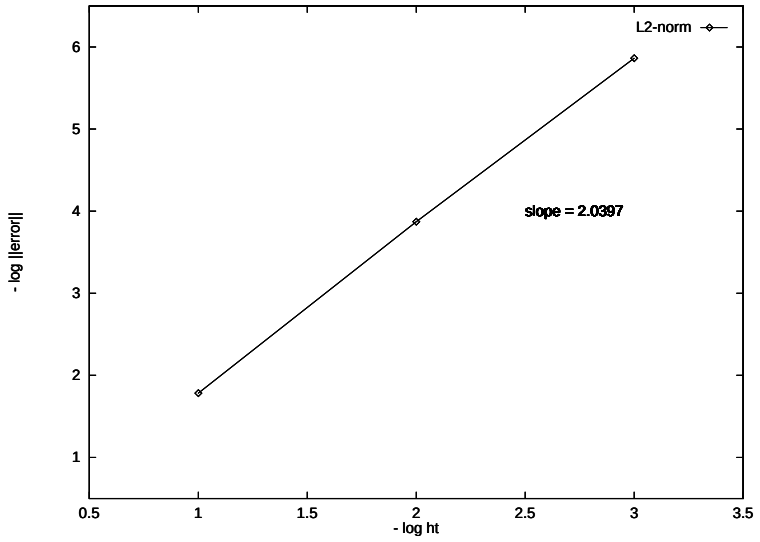

Figure 4.5: Rates of convergence for the concentration approximation in the L^2-norm using Crank-Nicolson method with 2×2 biquadratic elements

step sizes of 10^{-04} and 10^{-03}, respectively. Changes in nodal temperature and concentration are calculate with an input tolerance of 10^{-05}, and the calculations stop when the time is greater than 0.1.

We perform parametric studies of the PID controller for values similar to those used by Gustaffson et al. [11] and also by Coutinho and Alves [4]. We choose values of k_p ranging from 0.03 to 0.20, k_I from 0.03 to 0.40, and k_D from 0.003 to 0.02. Table 4.5 shows the L^2-norm of the error in the concentration solution, the number of time iterations, $ntstep$, the number of steps rejected, $nrejec$, for different values of the PID parameters, and the number total of Newton iterations, $newt$, and the computational effort, c_{effort}.

We can see from Table 4.5 that the error in the approximate solution at the final time is of order 10^{-06} for all cases studies. Moreover, with the PID control strategy we find approximate solutions with a much smaller number of time steps without any significant loss of accuracy. Observe that we need 100 time steps to obtain a solution with the same accuracy when the minimum fixed time step is used (Table 4.5).

The PID controller is very robust as we also can see from Table 4.5. Although feedback control theory provides techniques to choose the PID

case	k_p, k_I, k_D	error	*ntstep*	*nrejec*	*newt*	c_{effort}
1	0.05 0.05 0.005	.37023368E-05	66	0	132	0.66
2	0.1 0.3 0.015	.38890581E-05	62	0	124	0.62
3	0.075 0.175 0.01	.38512072E-05	62	0	124	0.62
4	0.1 0.16 0.011	.38680409E-05	63	0	126	0.63
5	0.06 0.13 0.008	.38456781E-05	63	0	126	0.63
6	0.08 0.216 0.0116	.38684855E-05	62	0	124	0.62
7	0.15 0.32 0.017	.38897674E-05	62	1	126	0.63
8	0.2 0.4 0.02	.38896720E-05	62	2	128	0.64
9	0.04 0.04 0.004	.36271440E-05	67	0	134	0.67
10	0.03 0.03 0.003	.35057604E-05	69	0	138	0.69
11	0.0 0.175 0.0	.38528566E-05	62	0	124	0.62
12	0.075 0.175 0.0	.38512100E-05	62	0	124	0.62
13	No control	.13711077E-05	100	0	200	1
14	Winget & Hughes	.32976399E-05	66	0	132	0.66

Table 4.5: Results for the PID controller using bilinear elements on a 2×2 grid.

parameters, robustness is required when a general finite element method is used for a wide range of different simulations. The variation in the number of time iterations is very small if we keep k_p in the range 0.05 to 0.10, k_I from 0.05 to 0.30, and k_D from 0.005 to 0.015.

Cases 3, 11, and 12 are plotted in Figures 4.6, 4.7 and 4.8, respectively. We also show results using the step size selection strategy developed by Winget and Hughes in Figure 4.9. This approach took 66 time steps with no rejected steps.

4.2 Isothermal Reaction on a Catalyst Slab

In this section we study an example of diffusion with homogeneous chemical reaction. Our objective is to validate our code with respect to the combined diffusion-reaction process. We discuss isothermal reaction inside a porous catalyst and compare our results with the studies performed by Finlayson [6] and Petersen [18].

When a catalyst particle made from a porous material impregnated with a

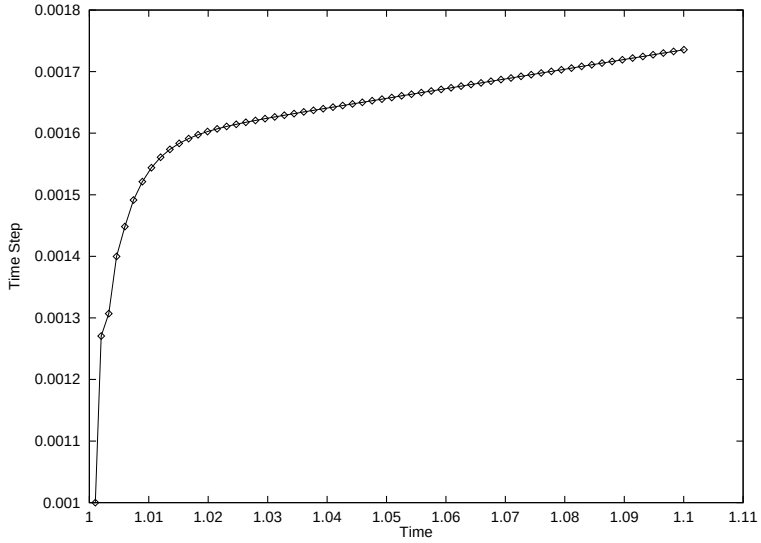

Figure 4.6: Time step variation for case 3 on a 2×2 grid using PID controller.

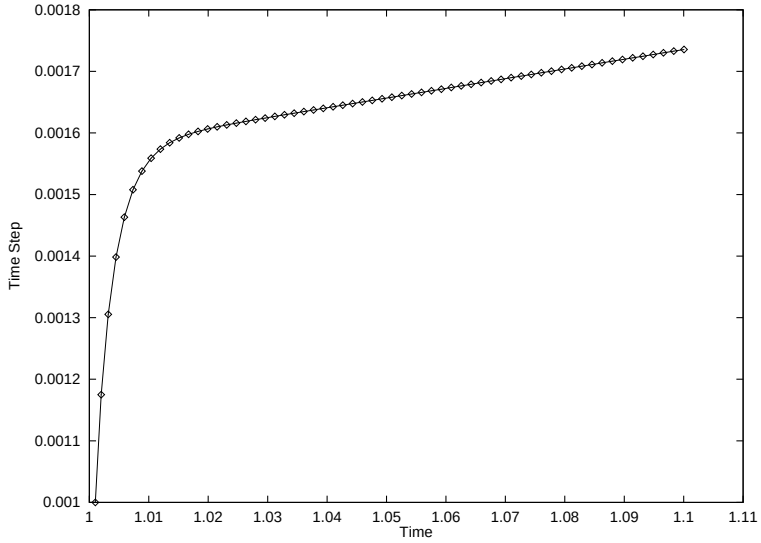

Figure 4.7: Time step variation for case 11 on a 2×2 grid using Integral Feedback controller.

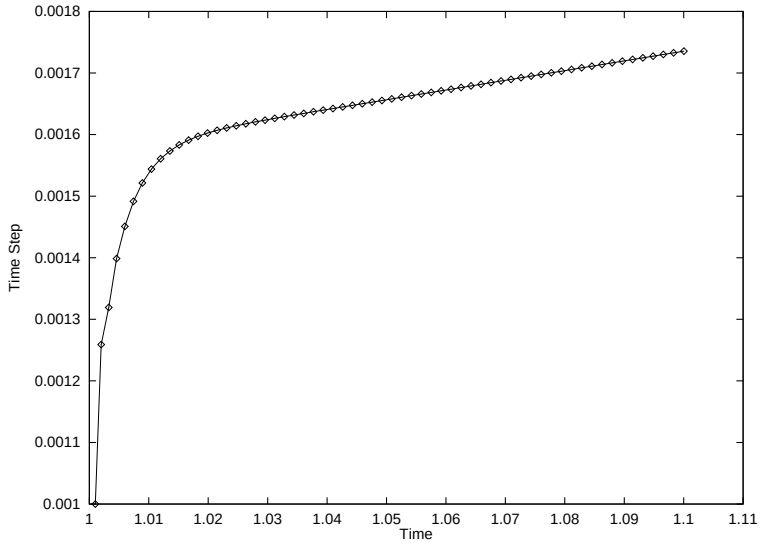

Figure 4.8: Time step variation for case 12 on a 2×2 grid using PI Feedback controller.

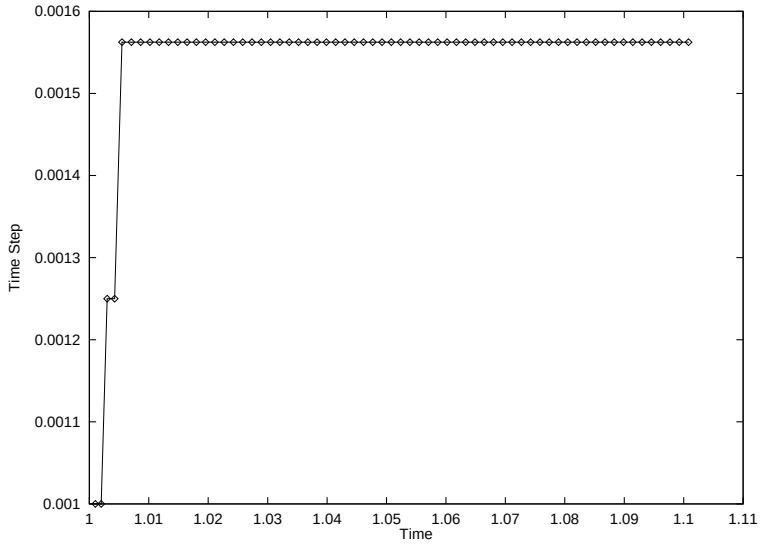

Figure 4.9: Time step variation on a 2×2 grid using Winget and Hughes approach.

catalytic substance is submerged in a gas stream, the reactant A diffuses into the particle, react on the catalytic surface, and the product B diffuses out, $A \rightarrow B$. We assume that the process is isothermal, i.e., the heat generated by the reaction can be neglected, and homogeneous, the chemical change takes places in the entire volume of the fluid. We also assume that the reaction mechanism is known.

Consider a catalyst section exposed to reactant A with concentration $\hat{c}$ at the surface. The rate of disappearance of reactant A is given by the following second-order, irreversible reaction

$$R = -kc^2$$

where c is the concentration of reactant A in the neighborhood of the surface, and k is a rate constant. The equations of the problem can be obtained applying the shell mass-balance method and Fick's first law to describe diffusion inside of a porous catalyst [1]. The equation of the problem is

$$\frac{\partial c}{\partial t} - \mathcal{D}\nabla^2 c = -kc^2 \tag{4.5}$$

with boundary conditions

$$-k\frac{\partial c}{\partial x} = 0 \text{ on } \partial\Omega - \partial\Omega_1 \tag{4.6}$$

$$c = \hat{c} \text{ on } \partial\Omega_1 \tag{4.7}$$

and initial condition

$$c(x, y, 0) = \hat{c}_0(x, y) \text{ in } \Omega \tag{4.8}$$

where $\mathcal{D}$ is the effective diffusivity measured experimentally, $\Omega = [0, L]\times[0, L]$ is the section, and $\partial\Omega_1$ is the right side of the domain.

The problem is scaled as follows: $x^*; y^* = x; y/L$, $t^* = t\mathcal{D}/L^2$, and $c^* = c/\hat{c}$. Substituting these relations into (4.5), (4.6), (4.7) and (4.8), we obtain the scaled form of the equations

$$\frac{\partial c^*}{\partial t^*} - \nabla^2 c^* = -\phi^2 c^{*2} \tag{4.9}$$

$$\frac{\partial c^*}{\partial x^*} = 0 \quad \text{on } \partial\Omega^* - \partial\Omega_1^* \tag{4.10}$$

$$c^* = 1 \quad \text{on } \partial\Omega_1^* \tag{4.11}$$

$$c^*(x^*, y^*, 0) = c_0(x^*, y^*) \quad \text{in } \Omega^* \tag{4.12}$$

where $\Omega^* = [0,1] \times [0,1]$ is the dimensionless section, $\partial\Omega_1^*$ is the right side of the domain, and ϕ is the Thiele modulus defined as

$$\phi = \sqrt{k\hat{c}L^2/\mathcal{D}}.$$

For convenience, we drop the superscript * henceforth.

We are interested on steady state solutions of the problem for different values of the Thiele modulus ϕ. We assume that the steady state occurs when

$$\|c^{n+1} - c^n\| < \tau_c \, \|c^{n+1}\|$$

where n denotes the timestep index, $\|\cdot\|$ denotes Euclidean norm, and τ_c is equal to 10^{-7} in this example. Since we are simulating a 1-D problem, we choose in all cases a mesh with 16×1 bilinear elements. We use the timestep control to calculate all approximate steady state solutions.

The effectiveness factor η gives the ratio of the amount reacted with diffusion to the amount that would be reacted if the concentration were everywhere the same, and equal to the value at the boundary. In this example, the effectiveness factor can be defined by the equation

$$\eta = \frac{\int_0^1 \phi^2 c^2 dx}{\int_0^1 \phi^2 1 dx}. \tag{4.13}$$

Finlayson [6] calculates approximate solutions for the problem on the interval [0,1] using the orthogonal collocation method. He shows that for one interior collocation point the effectiveness factor can be expressed by

$$\eta = \frac{1}{6} + \frac{5}{24} \frac{[-2.5 + (6.25 + 10\phi^2)^{1/2}]^2}{\phi^4}. \tag{4.14}$$

The approximation is accurate for $\phi \leq 2$, and for larger value of ϕ a higher approximation is required to improve the results. The effectiveness factor η is plotted versus the Thiele modulus ϕ in Figure 4.10 for the collocation method and Galerkin method. We can see that the two curves coincide for $\phi \leq 1.2$.

For large values of ϕ Petersen [18] shows that an asymptotic solution is available. In this case the general formula becomes

$$\eta = \sqrt{\frac{2}{3}} \frac{1}{\phi}. \tag{4.15}$$

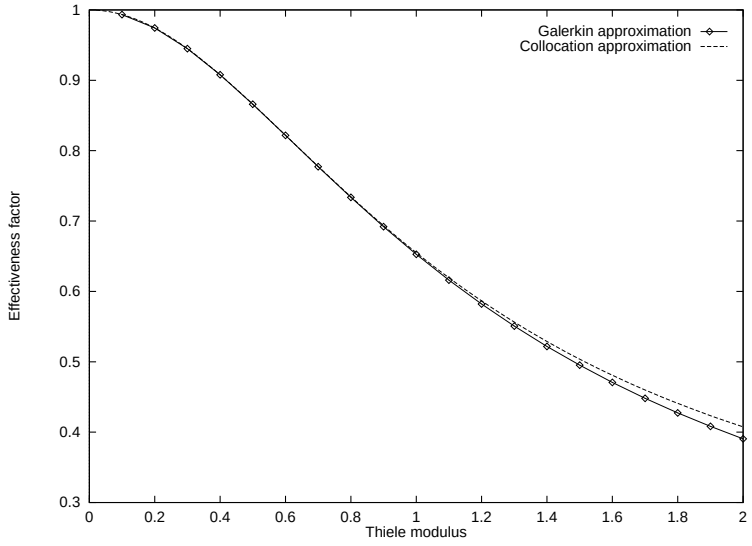

Figure 4.10: Effectiveness factor as a function of Thiele modulus for collocation method and Galerkin method.

Figure 4.11 shows the effectiveness factor η plotted against the Thiele modulus ϕ for values of $\phi \geq 3$. Observe that accurate solutions are also obtained for large values of ϕ. Consequently, the Galerkin formulation gives adequate approximations for all values of ϕ. The steady state solutions for different values of the Thiele modulus are shown in Figure 4.12.

4.3 Nonisothermal Reaction on a Catalyst Section

The problem studied now involves chemical reaction on a catalyst section with heat effects included. The process is highly nonlinear because of an exponential chemical reaction term arising from the temperature dependence of the chemical reaction rate. To obtain convergence of the Newton Raphson method used to solve the nonlinear system (2.26) resulting from the discretization in space of the transport equation by the finite element method, we need to choose a very small timestep. To increase the robustness of our time scheme, we use the timestep control studied before. We first consider an nonisothermal steady state case, then a time-dependent nonisothermal case.

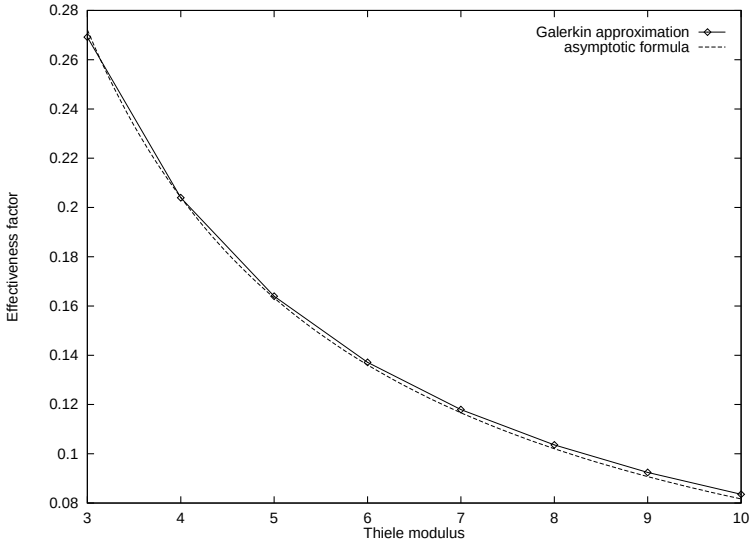

Figure 4.11: Effectiveness factor as a function of Thiele modulus for the asymptotic formula and Galerkin method.

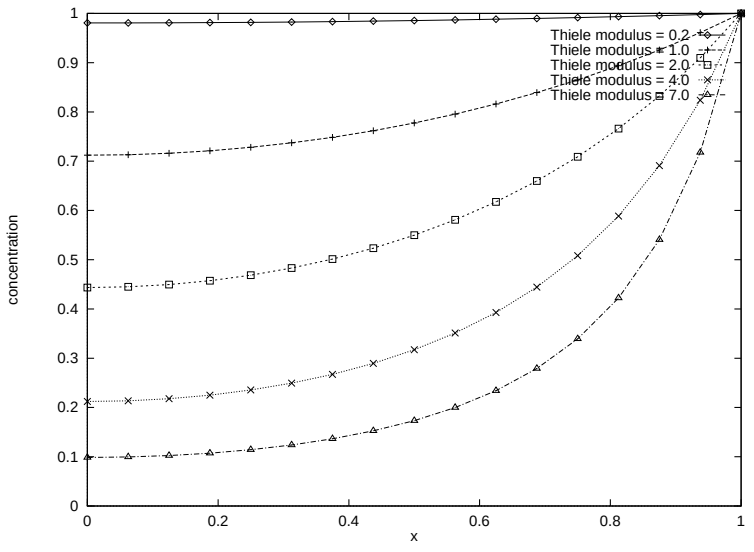

Figure 4.12: Steady state solution in catalyst for $\phi = 0.2$, 1.0, 2.0, 4.0 and 7.0.

Consider a first-order, irreversible reaction in a catalyst section $\Omega = [-L, L] \times [-L, L]$ with reaction rate given by

$$R = -a\, c\, \exp(-\Delta E/\hat{R}T),$$

where T is the absolute temperature, ΔE is the activation energy, $\hat{R}$ is the gas constant, and a is constant. The equations of the problem are

$$\begin{aligned} \rho c_p \frac{\partial T}{\partial t} + \rho c_p \mathbf{u} \cdot \nabla T - k\nabla^2 T &= a\, c\, \exp(-\frac{\Delta E}{\hat{R}T}) && (4.16) \\ \frac{\partial c}{\partial t} + \mathbf{u} \cdot \nabla c - \mathcal{D}\nabla^2 c &= -a\, c\, \exp(-\frac{\Delta E}{\hat{R}T}), && (4.17) \end{aligned}$$

with initial conditions

$$\begin{aligned} T(x, y, 0) &= \tilde{h}_1(x, y) \\ c(x, y, 0) &= \tilde{h}_2(x, y), \end{aligned} \qquad (4.18)$$

and boundary conditions

$$\begin{aligned} \frac{\partial T}{\partial n} &= \frac{\partial c}{\partial n} = 0 \quad \text{on } \partial\Omega_1 \\ -k\frac{\partial T}{\partial n} &= h_g(T - \tilde{T}) \quad \text{on } \partial\Omega_2 \\ -\mathcal{D}\frac{\partial c}{\partial n} &= k_g(c - \tilde{c}) \quad \text{on } \partial\Omega_2, \end{aligned} \qquad (4.19)$$

where ρ is the density, c_p is the specific heat, k is the thermal conductivity, $\mathcal{D}$ is the diffusivity, h_g is the heat transfer coefficient, k_g is the mass transfer coefficient, n is the unit outward normal, and $\partial\Omega = \partial\Omega_1 \cup \partial\Omega_2$ is the boundary of the domain.

The equations can be scaled as follows: $x^*; y^* = x; y\frac{1}{L}$, $u^*; v^* = u; v\frac{t_s}{L}$, $c^* = \frac{c}{c_0}$, $T^* = \frac{T}{T_0}$, and $t^* = \frac{t}{t_s}$. Substituting these relations into (4.16), (4.17), (4.18) and (4.19), we obtain the dimensionless unsteady equations for the non-isothermal problem

$$\begin{aligned} \frac{\partial T^*}{\partial t^*} + \mathbf{u}^* \cdot \nabla T^* - \frac{1}{M_1}\nabla^2 T^* &= \frac{\phi^2 c^* \beta}{M_1} \exp(\gamma(1 - \frac{1}{T^*})) && (4.20) \\ \frac{\partial c^*}{\partial t^*} + \mathbf{u}^* \cdot \nabla c^* - \frac{1}{M_2}\nabla^2 c^* &= -\frac{\phi^2 c^*}{M_2} \exp(\gamma(1 - \frac{1}{T^*})), && (4.21) \end{aligned}$$

with initial conditions

$$\begin{aligned} T^*(x,y,0) &= h_1(x,y) \\ c^*(x,y,0) &= h_2(x,y), \end{aligned} \tag{4.22}$$

and boundary conditions

$$\begin{aligned} \frac{\partial T^*}{\partial n} &= \frac{\partial c^*}{\partial n} = 0 \quad \text{on } \partial\Omega_1^* \\ -\frac{\partial T^*}{\partial n} &= \frac{Nu}{2}(T^* - g_1(t)) \quad \text{on } \partial\Omega_2^* \\ -\frac{\partial c^*}{\partial n} &= \frac{Sh}{2}(c^* - g_2(t)) \quad \text{on } \partial\Omega_2^*, \end{aligned} \tag{4.23}$$

where $M_1 = \rho c_p L^2/kt_s$, $M_2 = L^2/\mathcal{D}t_s$, $Nu = h_g 2L/\mathcal{D}$ is the Nusselt number, $Sh = k_g 2L/\mathcal{D}$ is the Sherwood number, $\phi = \sqrt{k_0 L^2/\mathcal{D}}$ is the Thiele modulus, $\Omega^* = [0,1] \times [0,1]$ is the dimensionless section, and $\partial\Omega^* = \partial\Omega_1^* \cup \partial\Omega_2^*$ is the boundary of the domain. Here $k_0 = a\exp(-\gamma)$. The dimensionless variables γ and β are defined as

$$\begin{aligned} \gamma &= \frac{\Delta E}{\hat{R}T_0}, \\ \beta &= \frac{(-\Delta H_R)c_0\mathcal{D}}{kT_0}, \end{aligned}$$

where $-\Delta H_R$ is the heat of reaction. For convenience, we drop the superscript * henceforth.

First we solve the nonisothermal case in steady state under conditions in which the Nusselt and Sherwood numbers are very large. The boundary conditions are

$$\begin{aligned} \frac{\partial T}{\partial n} &= \frac{\partial c}{\partial n} = 0 \quad \text{on } \partial\Omega_1 \\ T &= 1.1 \quad \text{on } \partial\Omega_2 \\ c &= 1.0 \quad \text{on } \partial\Omega_2 \end{aligned}$$

where $\partial\Omega_2$ is the right side of the unit square Ω, and $\partial\Omega_1 = \partial\Omega - \partial\Omega_2$. The functions h_1 and h_2 in (4.22) defining the initial conditions are

$$h_1(x,y) = h_2(x,y) = 1 + sin(\pi x)sin(\pi y).$$

The analytic solution for the Stokes problem is

$$\begin{aligned} u(x,y) &= 100x^2(1-x)^2(2y-6y^2+4y^3) \\ v(x,y) &= 100y^2(1-y)^2(-2x+6x^2-4x^3) \end{aligned} \tag{4.24}$$

where the viscosity $\nu = 0.01$, and the pressure is $p(x,y) = 100(x^2 - y^2)$. We calculate the approximate solution for the Stokes problem, substitute the velocities into the transport equation, and solve for the concentration and temperature of the problem. To find the velocity field we use biquadratic basis functions in a 4×4 grid with 2×2 point integration of the penalty term. Figure 4.13 shows the velocity for the Stokes problem.

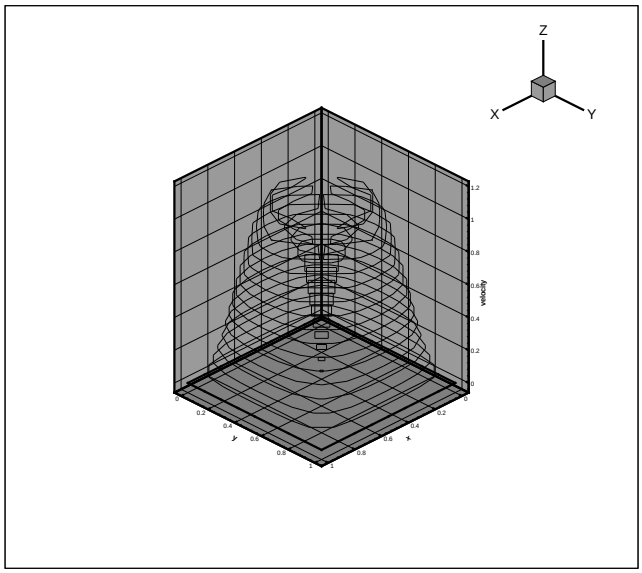

Figure 4.13: Velocity for Stokes flow.

We calculate the steady state approximate solution for the Thiele modulus $\phi = 0.8$, $\beta = 0.6$, $\gamma = 20$, $M_1 = 176$, $M_2 = 199$, and a grid with 8×8 bilinear elements. We assume that the steady state occurs when the following condition is satisfied

$$\frac{\|(\mathbf{T}^{m+1} - \mathbf{T}^m) + (\mathbf{c}^{m+1} - \mathbf{c}^m)\|}{\|\mathbf{T}^{m+1} + \mathbf{c}^{m+1}\|} < \tau$$

where m denotes the timestep index and $\|\cdot\|$ denotes Euclidean norm. The initial time step size is 10^{-03}, and the minimum and maximum time step sizes

allowed are 10^{-03} and 10, respectively. A tolerance of 10^{-04} was supplied for changes in nodal temperature and concentration, and $\tau = 10^{-04}$. We need to start with this small timestep to obtain convergence of the Newton sequence in the transport equation.

We perform parametric studies of the PID controller for values around those used by Gustaffson et al. [11] and also by Coutinho and Alves [4]. We choose values of k_p ranging from 0.03 to 0.20, k_I from 0.03 to 0.40, and k_D from 0.003 to 0.02.

Table 4.6 shows for different values of the PID parameters the number of time iterations, *ntstep*, the number of steps rejected, *nrejec*, the number of Newton iterations, *newt*, and the computational effort, c_{effort}. We need about 800 Newton iterations to obtain the solution applying the PID control, in contrast with 2998 Newton iterations (case 10) when a fixed timestep is used. We have in this example a 3.75 times improvement in the computational effort to compute the solution within the same accuracy.

case	k_p, k_I, k_D	*ntstep*	*nrejec*	*newt*	c_{effort}
1	0.075 0.175 0.01	240	7	800	0.27
2	0.1 0.3 0.015	232	11	792	0.26
3	0.05 0.05 0.005	282	1	897	0.30
4	0.1 0.16 0.011	242	7	807	0.27
5	0.06 0.13 0.008	247	6	819	0.27
6	0.08 0.216 0.0116	237	9	800	0.27
7	0.2 0.4 0.02	229	14	791	0.26
8	0.03 0.03 0.003	315	0	981	0.33
9	0.0 .175 0.0	241	8	807	0.27
10	No Control	1101	0	2998	1
11	Winget & Hughes	264	8	876	0.29

Table 4.6: Results for the PID timestep controller and Winget & Hughes approach

The PID control is robust since the number of Newton iterations does not change too much for the different values of the PID parameters. We can also observe that the number of rejected timesteps is relatively small. The results for Winget and Hughes approach [21] are presented in case 11. The PID controller find the steady state solution a little faster than Winget and

Hughes approach. Figure 4.14 and 4.15 show the timestep size against time for case 1 and Winget and Hughes approach, respectively. We can observe that the PID control produces a very smooth curve. The initial temperature profile and the steady state solution are shown in Figure 4.16.

Next we solve the unsteady problem (4.20), (4.21), (4.22) and (4.23) with $M_1 = 176$, $M_2 = 199$, $Nu = 55.3$, $Sh = 66.5$, $\gamma = 20$, $\beta = 0.6$, and $\phi = 0.8$. The velocity field is the same calculated in the steady state problem (Figure 4.13). The approximate solutions are calculated using a grid with 8×8 bilinear elements. We first obtained the approximate solution for a constant timestep size of $\Delta t = 0.05$. Figure 4.17 shows the transient temperature distribution in a catalyst section at times t = 0, 1, 5, 10 and 20.

For a fixed time equal to 20, we compare approximate solutions using the PID controller and Winget and Hughes approach. We start with a timestep size of 0.05, and we allow minimum and maximum time steps of 0.05 and 5, respectively. The solutions are obtained with a tolerance of 10^{-06} for the changes in nodal temperature and concentration. The PID parameters are $k_p = 0.075$,$k_i = 0.175$ and $k_d = 0.01$.

Table 4.7 shows the results for each case studied. We obtain the solution with 423 Newton iterations using the PID controller, and we need 1223 Newton iterations with a fixed timestep of 0.05. Thus, we have obtained this solution 2.89 times faster. Here we also obtain the solution using the PID controller a little faster than using Winget and Hughes approach. Figure 4.18 and 4.19 show the timestep size against time for the PID controller and Winget and Hughes approach, respectively.

case	$ntstep$	$nrejec$	$nnewt$	c_{effort}
No Control	400	0	1223	1
PID Control	104	1	423	0.34
Winget&Hughes	112	1	433	0.35

Table 4.7: Results for the transient catalyst problem with timestep control and Winget and Hughes approach.

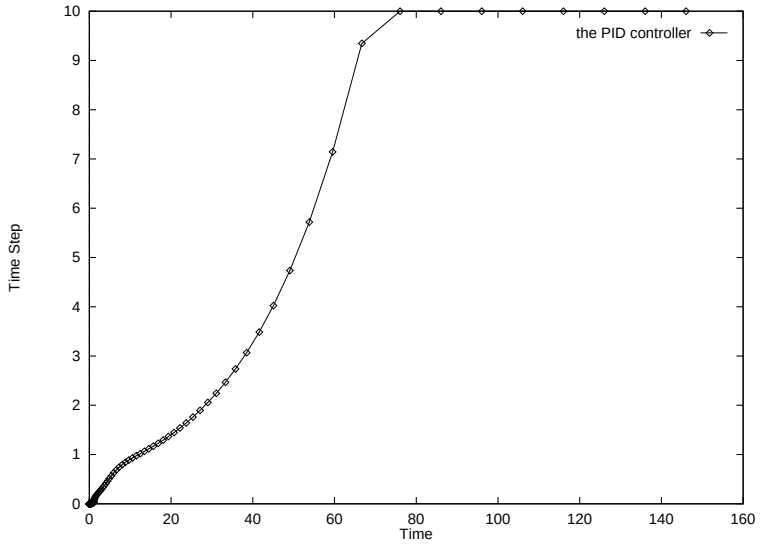

Figure 4.14: Timestep variation using the PID controller for case 1 (steady state problem).

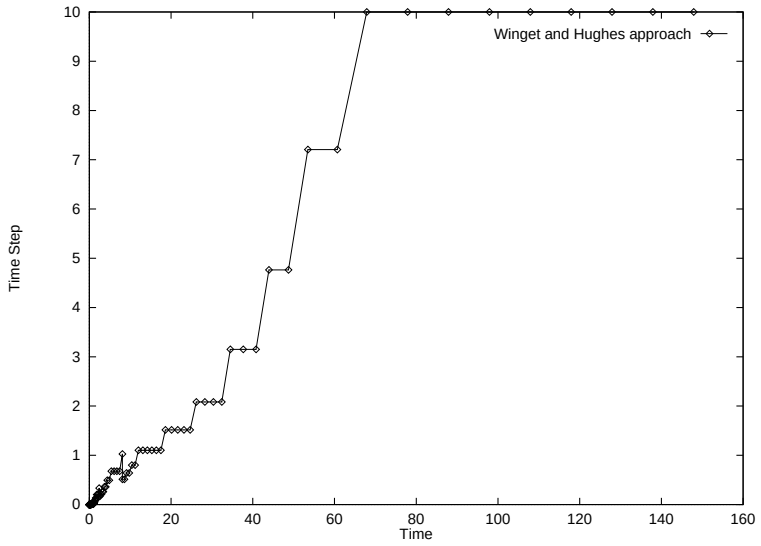

Figure 4.15: Timestep variation using Winget and Hughes approach (steady state problem).

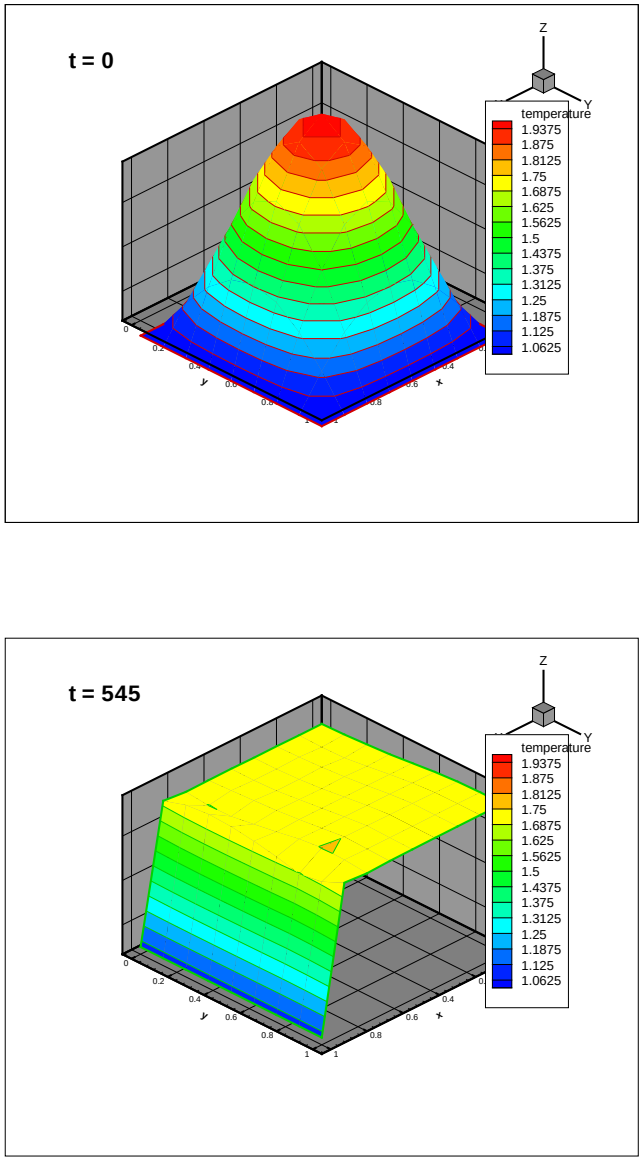

Figure 4.16: Initial temperature profile and steady state solution using bilinear elements on a 8×8 grid ($\phi = 0.8$).

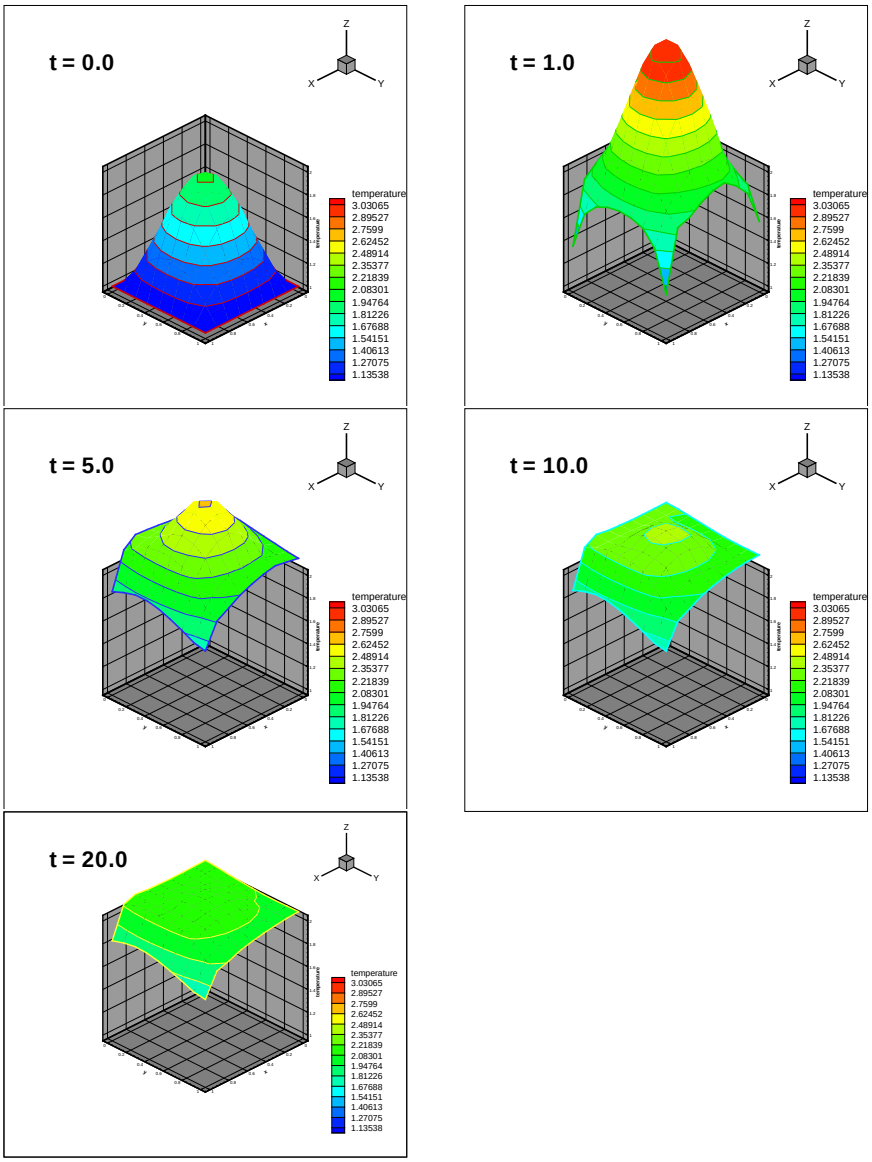

Figure 4.17: Evolution of temperature solution using bilinear elements on a 8×8 grid

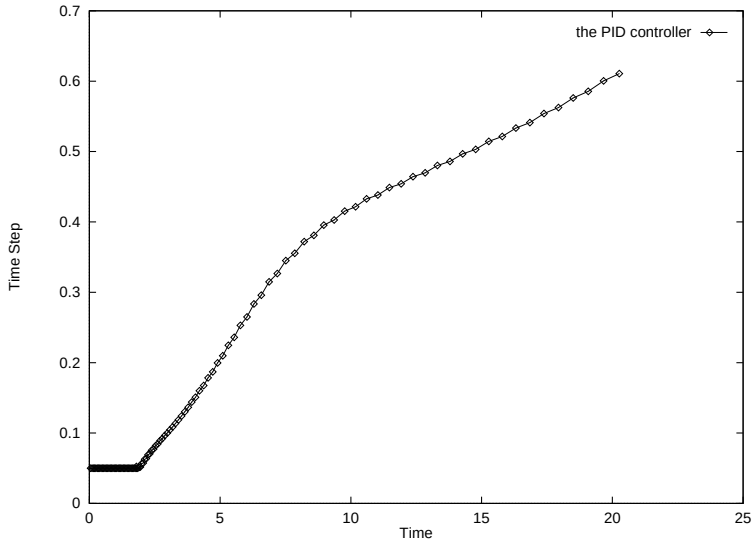

Figure 4.18: Timestep variation using the PID controller (transient problem).

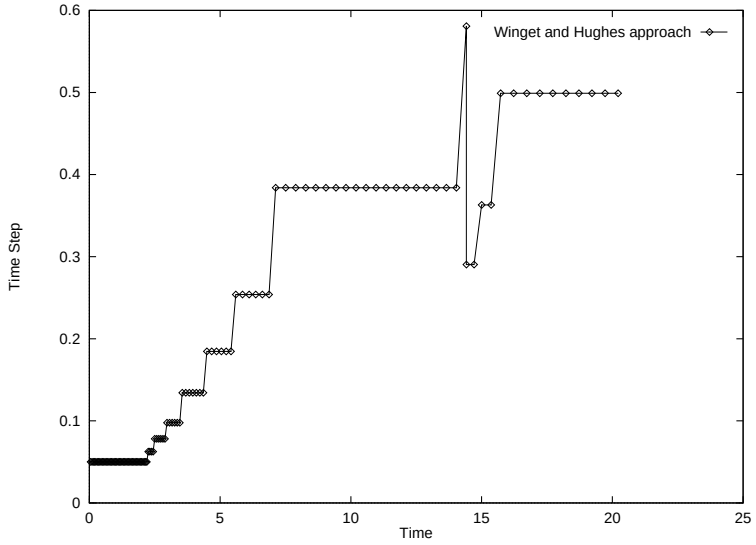

Figure 4.19: Timestep variation using Winget and Hughes approach (transient problem).

4.4 Boundary Control Application

To test our boundary control, we solve the nonisothermal problem (4.20) and (4.21) in steady state with initial condition

$$\begin{aligned} T(x,y,0) &= (1+cos(\pi/2x))\,bc \\ c(x,y,0) &= 1+cos(\pi/2x) \end{aligned}$$

and boundary conditions

$$\begin{aligned} \frac{\partial T}{\partial n} &= \frac{\partial c}{\partial n} = 0 \quad \text{on } \partial\Omega_1 \\ T &= bc \quad \text{on } \partial\Omega_2 \\ c &= 1.0 \quad \text{on } \partial\Omega_2 \end{aligned}$$

where $\partial\Omega_2$ is the right side of the unit square Ω, $\partial\Omega_1 = \partial\Omega - \partial\Omega_2$, and bc is the imposed temperature on the boundary $\partial\Omega_2$ update at each step of the boundary control. The constants of the problem are: $\phi = 0.2$, $\beta = 0.6$, $\gamma = 20$, and $M_1 = M_2 = 1.0$. The velocity field is zero, $u = v = 0$. The target solution is the approximate solution of the problem with $bc = 1.0$ on $\partial\Omega_2$, i.e., $T = 1.0$ on $\partial\Omega_2$. The target value, c_{targ}, is the target temperature at the middle of the domain, $c_{targ} = 1.5283911$.

The PID constants of the boundary control are $k_p = 0.05$, $k_i = 0.175$, $k_d = 0.01$, $\delta bc_m = 0.1$, and we stop the process when $\epsilon = 10^{-02}$. The steady state solutions are calculated using the timestep control proposed here, and a grid with 8×8 bilinear elements. First, we start the boundary control process with $bc_m = 0.3$ (Case 1) and, then with $bc_m = 1.2$ (Case 2).

Figure 4.20 and Figure 4.21 show the values of the temperature on $\partial\Omega_2$ calculate by the boundary control at each iteration for Cases 1 and 2, respectively. The final value of bc_{m+1} obtained by the boundary control is 1.0063 with $m = 13$ in Case 1, and 1.0060 with $m = 27$ in Case 2. The approximate steady state temperature and concentration in catalytic for $y = 1.0$ (Case 1) with the correspondent target solution are shown in Figures 4.22 and 4.23, respectively.

We observe that the control works correctly in both cases. However, the controller do not produce a smooth sequence of boundary steps and oscillates too much around the target solution. We can observe in both cases that the boundary control produces excessive growth and reduction of the boundary step after it gets closer to the target solution. We have not defined here

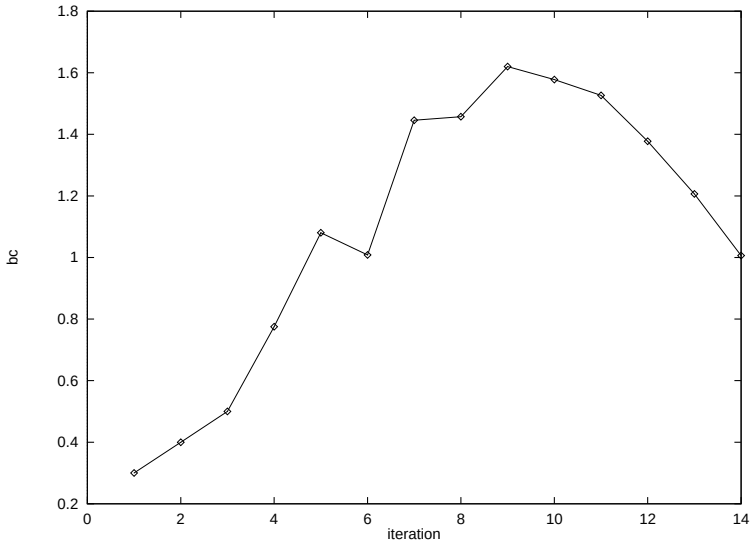

Figure 4.20: The temperature on the boundary for each iteration of the boundary control (Case 1).

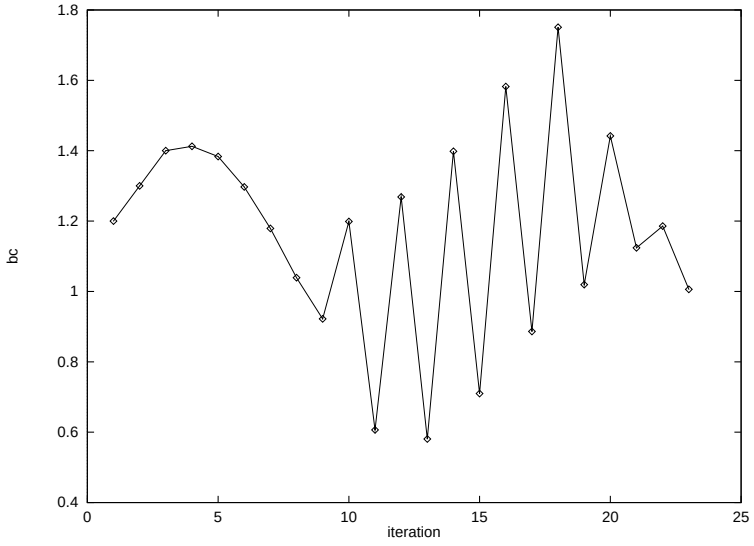

Figure 4.21: The temperature on the boundary for each iteration of the boundary control (Case 2).

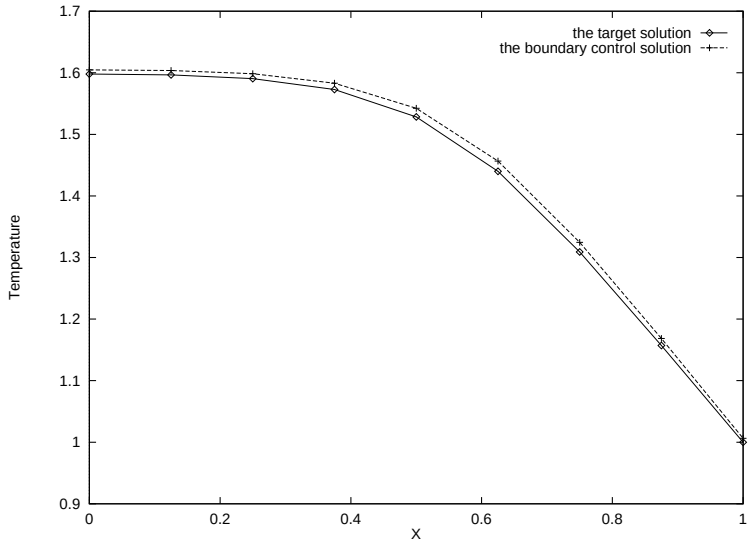

Figure 4.22: The steady state temperature for $y = 1.0$ calculate using the boundary control and the target temperature (Case 1).

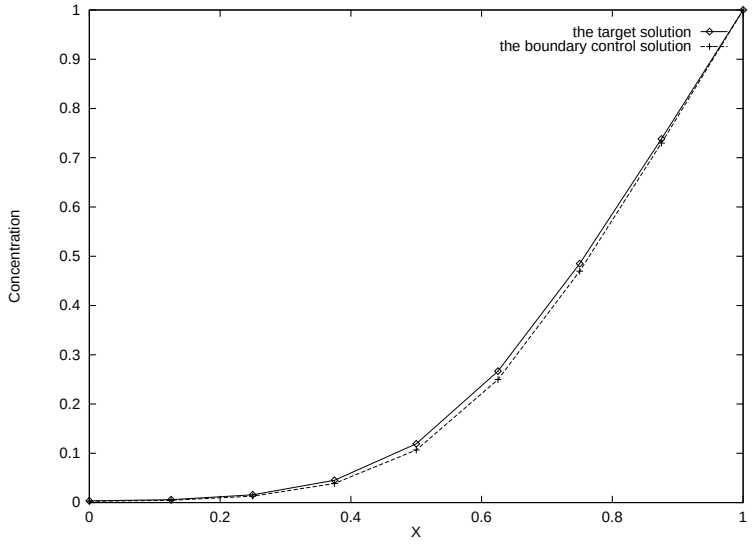

Figure 4.23: The steady state concentration for $y = 1.0$ calculate using the boundary control and the target concentration (Case 1).

boundary step limiters. Setting a maximum boundary step of 0.3 in Case 1, we can reduce the number of steps of the boundary control from 14 to 6, see Figure 4.24.

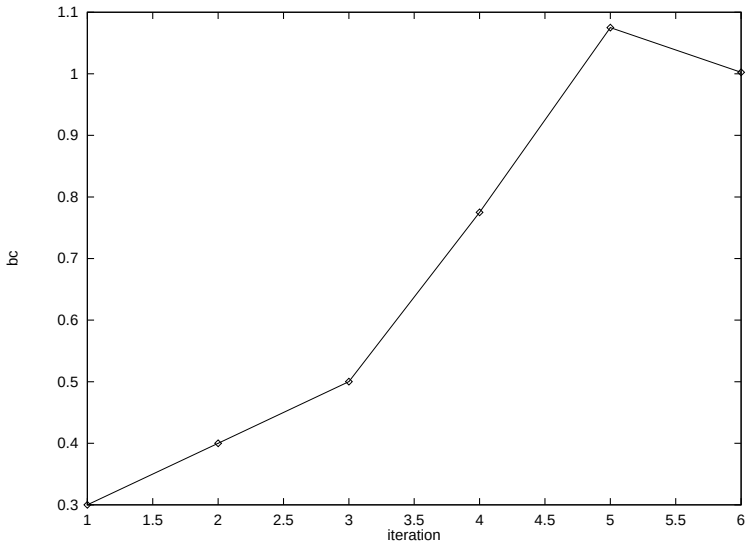

Figure 4.24: The temperature on the boundary for each iteration of the boundary control.

Chapter 5

Conclusions

We introduced an adaptive timestep selection scheme based on feedback control theory to increase the robustness of our finite element formulation of coupled incompressible viscous flow and nonlinear transient heat and mass transfer. Our finite element flow formulation is based on a penalty Galerkin method and the nonlinear reactive transport application utilizes a Galerkin approach. The algorithm employs an iteratively decoupled scheme in the present work.

We solve a representative test problem for 2D coupled viscous flow and reactive transport, and results are compare with fixed timestep, an adaptive timestep scheme from the literature, and our PID control approach. We also studied a highly nonlinear process involving chemical reaction on a catalyst section with heat effects included.

With the PID control strategy we find approximate solutions with a much smaller number of steps without any significant loss of accuracy. For instance, we have a 3.75 times improvement in the computational effort to compute the solution within the same accuracy in the nonisothermal reaction problem of Section 4.3. Some promising results with PID control for timestep selection, such as, smooth variation in timestep suggest that a robust algorithm is possible.

We design a PID controller to solve a simple chemically reacting system through automatic feedback control applied to the boundary conditions. No attempt is made to design an optimal feedback control law. The PID boundary control shows inefficient at present - others approaches like optimization appear preferable.

Bibliography

[1] R.B. Bird, W.E. Stewart, and E.N. Lightfoot. *Transport Phenomena.* John Wiley & Sons, New York, NY, 1960.

[2] G.F. Carey and R. Krishnan. Penalty approximation of stokes flow. *Comput. Meths. Appl. Mech. Engrg.*, 35:169–206, 1982.

[3] G.F. Carey and J.T. Oden. *Finite Elements: Fluid Mechanics*, volume 6. Prentice–Hall, Englewood Cliffs, NJ, 1986.

[4] A.L.G.A. Coutinho and J.L.D. Alves. Parallel finite element simulation of miscible displacements in porous media. *SPE Journal*, 4(1):487–500, 1996.

[5] R.C. Dorf and R.H. Bishop. *Modern Control Systems.* Addison-Wesley Publishing Company, 1995.

[6] B.A. Finlayson. *The Method of Weighted Residuals and Variational Principles*, volume 87 of *Mathematics in Science and Engineering.* Academic Press, New York, NY, 1972.

[7] J.D. Powell G.F. Franklin and A. Emami-Naeini. *Feedback Control of Dynamic Systems.* Addison-Wesley Publishing Company, 1994.

[8] W.R. Graham, J. Peraire, and K.Y. Tang. Optimum control of vortex shedding using low order models part i: Open-loop model development. *Internat. J. Numer. Meth. Eng.*, 87:281–304, 1997.

[9] W.R. Graham, J. Peraire, and K.Y. Tang. Optimum control of vortex shedding using low order models part ii: Model-based control. *Internat. J. Numer. Meth. Eng.*, 87:281–304, 1997.

[10] M.D. Gunzburger and H.C. Lee. Feedback control of karman vortex shedding. *Journal of Applied Mechanics*, 63:828–835, September 1996.

[11] K. Gustafsson, M. Lundh, and G. Söderlind. A pi stepsize control for the numerical solution for ordinary differential equations. *BIT*, 28:270–287, 1988.

[12] E. Hairer and G. Wanner. *Solving Ordinary Differential Equations II: Stiff and Differential-Algebraic Problems.* Springer–Verlag, 1993.

[13] B.P. Jacob and N.F.F. Ebecken. Adaptative time integration of nonlinear structural dynamic problems. *Eur. J. Mech*, 12(2):277–298, 1993. A/Solids.

[14] Z. Johan, T.J.R. Hughes, and F. Shakib. A globally convergent matrix-free algorithm for implicit time-marching schemes arising in finite element analysis in fluids. *Comp. Meth. Appl. Mech. Engng.*, 87:281–304, 1991.

[15] C. Johnson and J. Pitkaranta. Analysis of some mixed finite elements related to reduced integration. Technical report, Chalmers University of Technology and University of Göteborg, Göteborg, Sweden, 1980.

[16] D.S. Malkus and J.R. Hughes. Mixed finite element methods - reduced and selective integration techniques: A unification of concepts. *Comp. Meth. Appl. Mech. and Eng.*, 15:63–81, 1978.

[17] D.S. Park, D.M. Ladd, and E. Hendricks. Feedback control of karman vortex shedding. *ASME*, 38:59–64, 1992.

[18] E.E. Petersen. *Chemical Reaction Analysis.* Prentice–Hall, Englewood Cliffs, NJ, 1965.

[19] Y.J. Song, J.T. Oden, and N. Kikuchi. Discrete lbb-conditions for rip-finite element methods. Technical report, TICOM Report 80, The Texas Institute for Computational Mechanics, Austin, Texas, 1980.

[20] K.Y. Tang, W.R. Graham, and J. Peraire. Active flow control using a reduced order model and optimum control. *American Institute of Aeronautics and Astronautics*, 87:281–304, 1996.

[21] J.M. Winget and T.J.R. Hughes. Solution algorithms for nonlinear transient heat conduction analysis employing element-by-element iterative strategies. *Comp. Meth. Appl. Mech. and Eng.*, 52:711–815, 1985.

[22] O.C. Zienkiewicz. *The Finite Element Method.* McGraw-Hill, U.K., 1977.